The Role of Ferroptosis in Breast Cancer Metastasis

Adela Valentova

Linacre College



Department of Oncology

University of Oxford

A thesis submitted for the degree of

MSc by Research in Oncology

Word count: 12728

Michaelmas 2025

Abstract

Metastatic breast cancer remains a major clinical challenge, driven by molecular adaptations that promote therapy resistance and immune evasion. This study investigated ferroptosis, an iron-dependent form of regulated cell death, in lung- and bone-metastatic sublines of MDA-MB-231 breast cancer cells. RNA sequencing revealed downregulation of antigen presentation and ferroptosis defence pathways in metastatic cells. Functional assays confirmed reduced MHC-I expression coupled with impaired T-cell activation alongside increased lipid peroxidation, intracellular iron accumulation, and heightened sensitivity to ferroptosis induction. *In vivo* pilot studies demonstrated that metastatic tumour cells exhibited increased primary tumour growth rates. Treatment with a ferroptosis inducer resulted in increased lipid peroxidation and modulation of MHC-I. However, this did not translate into a measurable therapeutic effect, likely due to pharmacological limitations. Collectively, these findings identify immune evasion alongside ferroptosis vulnerability as a potential therapeutic target in metastatic breast cancer and point to a broader capacity for immune modulation. This work provides a foundation for future studies exploring ferroptosis-based strategies to overcome metastatic disease.

Acknowledgements

I would like to express my sincere gratitude to my primary supervisor, Dr. Ejung Moon, for her guidance and support throughout this project, and for helping me grow into the researcher I am today. Her encouragement consistently pushed me to do my best and develop both my skills and confidence. I am especially grateful to my secondary supervisor, Dr. Nuria Vilaplana Lopera, without whom this work would not have been possible; she trained me in most of the techniques and generously shared her expertise, and I am fortunate to count her not only as a mentor but also as a friend. I would also like to thank the rest of the lab, Pei Ju Lee and Jiyoung Kim, for their advice and encouragement, and Tianxu Hou, who shared the Master's programme with me, for making the experience so enjoyable. I extend a special thanks to Dr. Ahmet Hazini for providing materials and advice that were invaluable for the antigen presentation aspect of my project. My thanks also go to Dr. Hala Estephan and Edward Petrosyan for their support and friendship throughout my Master's, and for the many enjoyable lunches shared with the lab. Finally, I am deeply grateful to my family, with special thanks to my mum for her unwavering encouragement, as well as to all my friends, especially Sophie and Jennie, for being there for me throughout this year, and to my partner Daniel for being by my side every day.

Table of Contents

Abstract ..... *I*

Acknowledgements ..... *II*

List of Abbreviations ..... *V*

Introduction *1*

Breast cancer metastasis **1**

Lung and bone niches **3**

Stress adaptations **5**

Ferroptosis **6**

Antigen presentation **9**

Study aims **10**

Materials and Methods *12*

Tissue Culture **12**

Reagents **12**

T Cell Activation Assay **13**

Cell Viability Assay **13**

FerroOrange Assay **14**

Immunofluorescence Staining **14**

Flow Cytometry **15**

Live Cell Staining for Lipid Peroxidation and Lipid Droplets 15

Antibody-Based Cell Surface Staining 15

Western Blotting **16**

Protein Extraction and Quantification 16

Sample Preparation and Gel Electrophoresis 16

Protein Transfer and Blocking 17

Antibody Incubation and Detection 17

***In vivo* Studies** **18**

Immunohistochemistry (IHC) **19**

Processing, Embedding, and Sectioning 19

Deparaffinisation and Rehydration 19

Antigen Retrieval and Blocking 19

Primary and Secondary Antibody Incubations 19

Detection and Counterstaining 20

Iron Staining 20

Bone Tissue Microarray 21

IHC analysis 21

RNA-Sequencing Analysis **22**

Statistical Analysis **22**

Results *23*

Suppressed ferroptosis defence and antigen presentation in metastasis **23**

Metastatic cells exhibit increased sensitivity to ferroptosis 27
Ferroptosis induction increases MHC-I expression in metastatic cells 31
Ferroptosis modulates lipid peroxidation and antigen presentation in metastatic tumours ... 34
Discussion 38
Molecular characteristics of metastatic breast cancer cells 39
Enhanced ferroptosis sensitivity in metastatic sublines 40
Ferroptosis induction and modulation of antigen presentation 44
Ferroptosis induction alters lipid peroxidation and antigen presentation *in vivo* 46
Therapeutic implications 49
Limitations and future directions 50
Conclusion 52
Appendix A: Individual enrichment plots for LM and BoM sublines 53
Appendix B: H&E staining of lungs from IKE-treated and control mice 54
H&E staining reveals lung metastases in control and IKE-treated mice 54
Method 54
References 56

List of Abbreviations

Abbreviation	Full Term
ACSL4	Acyl-CoA Synthetase Long-Chain Family Member 4
15-LOX	15-Lipoxygenase
αMEM	Alpha Minimum Essential Medium
ANOVA	Analysis of Variance
ARE	Antioxidant Response Element
BACH1	BTB and CNC homology 1
BoM	Bone Metastatic
BODIPY	Boron-dipyrromethene
CA9	Carbonic Anhydrase IX
DAB	Diaminobenzidine
DMEM	Dulbecco's Modified Eagle Medium
DPBS	Dulbecco's Phosphate-Buffered Saline
EDTA	Ethylenediaminetetraacetic Acid
EMT	Epithelial–Mesenchymal Transition
FACS	Fluorescence-Activated Cell Sorting
FBS	Foetal Bovine Serum
GFP	Green Fluorescent Protein
GPX4	Glutathione Peroxidase 4
GSH	Glutathione
GSSH	Glutathione Disulfide
H&E	Haematoxylin and Eosin
HEPES	4-(2-hydroxyethyl)-1-piperazineethanesulfonic acid

Abbreviation	Full Term
HER2	Human Epidermal Growth Factor Receptor 2
HIF-1α	Hypoxia-Inducible Factor 1 Alpha
HLA	Human Leukocyte Antigen
HLA-ABC	Pan-classical MHC-I molecules (HLA-A, HLA-B, HLA-C)
HLA-A2	Human Leukocyte Antigen, A2 allele
HLA-E	Human Leukocyte Antigen, E allele
IC_{50}	Half maximal inhibitory concentration
IHC	Immunohistochemistry
IKE	Imidazole Ketone Erastin
IL-11	Interleukin-11
Ki67	Proliferation Marker Ki67
LM	Lung Metastatic
LPCAT3	Lysophosphatidylcholine Acyltransferase 3
MHC-I	Major Histocompatibility Complex Class I
NAT	Normal Adjacent Tissue
NFAT	Nuclear Factor of Activated T Cells
NY-ESO-1	New York Esophageal Squamous Cell Carcinoma 1
PARP	Poly (ADP-ribose) Polymerase
PD-L1	Programmed Death-Ligand 1
PE	Phosphatidylethanolamine
PTHrP	Parathyroid Hormone-Related Protein
PUFA	Polyunsaturated Fatty Acid
RANKL	Receptor Activator of Nuclear Factor κB Ligand

Abbreviation	Full Term
RPMI	Roswell Park Memorial Institute Medium
RT	Room Temperature
SD	Standard Deviation
TFR1	Transferrin Receptor 1
TMA	Tissue Microarray
TNBC	Triple-Negative Breast Cancer
VEGF	Vascular Endothelial Growth Factor
WT	Wild Type
ICD	Immunogenic Cell Death
DAMP	Damage-Associated Molecular Pattern
ROS	Reactive Oxygen Species
PUFA-PE	Phosphatidylethanolamine-bound Polyunsaturated Fatty Acid
PUFA-PE-OOH	Oxidised Phosphatidylethanolamine-bound PUFA
RSL3	Ras-selective lethal small molecule 3
ZEB1	Zinc finger E-box-binding homeobox 1
NSG	NOD scid gamma (NOD.Cg-Prkdcscid Il2rgtm1Wjl/SzJ)
FADS1	Fatty acid desaturase 1
FADS2	Fatty acid desaturase 2
MUFA	Monounsaturated fatty acid
DMSO	Dimethyl sulfoxide
DAPI	4′,6-diamidino-2-phenylindole
HMGB1	High mobility group box 1
BRCA	Breast cancer gene (BRCA1/2)

Abbreviation	Full Term
FITC	Fluorescein isothiocyanate
FOXC2	Forkhead box protein C2
CXCL1	C-X-C motif chemokine ligand 1
CXCR4	C-X-C chemokine receptor type 4
MMP1	Matrix metallopeptidase 1
NOD	Non-obese diabetic (mouse strain background)

Introduction

Breast cancer metastasis

Breast cancer remains one of the most prevalent cancers worldwide and a leading cause of cancer-related mortality (World Health Organization, 2025). In 2022, approximately 2.3 million women were diagnosed with breast cancer globally, resulting in around 670,000 deaths, the majority of which are attributable to metastatic disease (Kim et al., 2025). As global incidence continues to rise, there is an urgent need to develop innovative therapeutic strategies that more effectively target metastatic disease (Siegel et al., 2025).

Breast cancer is a heterogeneous disease that can be divided into subtypes with distinct biological and clinical features (Wu et al., 2022). Most cases are invasive carcinomas (around 70–75%), while invasive lobular carcinomas make up 12–15%, with the rest being a range of rarer forms (Tan et al., 2020). Subtyping is guided by histology and immunohistochemistry, including the evaluation of hormone receptors (oestrogen and progesterone), human epidermal growth factor receptor 2 (HER2) status, and the proliferation marker Ki67 (Burstein et al., 2021). On this basis, tumours are broadly classified into three major groups: hormone receptor–positive/HER2-negative (~70%), HER2-positive (15–20%), and triple-negative breast cancer (TNBC, ~15%) (Burstein et al., 2021, Waks and Winer, 2019). In clinical practice, these categories are further refined into four recognised subtypes. Luminal A cancers show strong hormone receptor expression with low Ki67, and generally grow more slowly, have better outcomes, and respond well to endocrine therapies (Burstein et al., 2021, Waks and Winer, 2019). Luminal B cancers also express hormone receptors but have higher proliferative activity and can be either HER2-positive or negative, often requiring chemotherapy in addition to hormone therapy (Burstein et al., 2021, Waks and Winer, 2019). HER2-enriched tumours, defined by high HER2 expression, are typically more aggressive but respond to HER2-targeted treatments

(Burstein et al., 2021). Triple-negative breast cancer (TNBC) lacks expression of oestrogen and progesterone receptors as well as HER2, making it unresponsive to targeted therapies used in other breast cancer subtypes (Burstein et al., 2021, Waks and Winer, 2019). It is a biologically aggressive disease, most commonly presenting as high-grade, highly proliferative invasive ductal carcinomas (Geyer et al., 2017). Systemic chemotherapy remains the mainstay of treatment, with poly-ADP ribose polymerase (PARP) inhibitors available for patients with germline *BRCA* gene mutations and immunotherapy showing benefit only in select subsets (Cardoso et al., 2019, Gradishar et al., 2022, Litton et al., 2018, Robson et al., 2017, Kwa and Adams, 2018, Wu et al., 2024). TNBC is associated with early relapse and frequent metastasis to distant organs, underscoring its poor prognosis and the urgent need for innovative strategies to more effectively target metastatic disease (Dent et al., 2007, Lin et al., 2012).

Metastasis is a multistep process in which tumour cells escape the primary site and colonise distant organs. One important route is via angiogenesis, where newly formed tumour-associated blood vessels are abnormal, excessively branched, and leaky, thereby facilitating tumour cell intravasation (Weidner et al., 1991, Fukumura and Jain, 2008). This vascular malformation arises from dysregulated angiogenic signalling, such as elevated vascular endothelial growth factor A (VEGF-A) expression, and produces regions of hypoxia and acidosis within the tumour (Kim et al., 1993). Such conditions impair immune surveillance and drug delivery, while the activation of an “angiogenic switch” promotes renewed tumour growth and dissemination (Maeda, 2001, Folkman, 2002). In addition to blood vessels, tumour cells can spread through lymphatic and perineural routes to distant organs, processes supported by VEGF-C/VEGF-D–driven lymphangiogenesis and immune-modulating signals in the tumour microenvironment (Zhang et al., 2020, Mandriota et al., 2001, Karaman and Detmar, 2014). To survive in the circulation and invade new tissues, cancer cells often undergo epithelial–mesenchymal transition (EMT), a developmental program that reduces cell–cell adhesion and confers invasive, migratory,

and stem-like properties (Klymkowsky and Savagner, 2009, Polyak and Weinberg, 2009). EMT is driven by transcription factors such as forkhead box protein C2 (FOXC2), Twist, Snail, and Zinc finger E-box-binding homeobox (ZEB) proteins, which rewire signalling pathways to promote plasticity and resistance, driving the acquisition of migratory traits (Mani et al., 2007, Yang et al., 2004, Cano et al., 2000, Taube et al., 2010). Dissemination can then proceed through either single-cell invasion, requiring cytoskeletal remodelling and protease activity, or collective migration, in which leader and follower cells cooperate to remodel the extracellular matrix (Winkler et al., 2020, Zhang et al., 2019a). These processes ultimately allow tumour cells to survive the stresses of circulation, evade immune detection, and dynamically interact with host cells and systems, all while adapting to foreign microenvironments (de Visser and Joyce, 2023, Kamińska et al., 2015, Seager et al., 2017). Adaptations, not only enable colonisation, but also complicate treatment and contribute to the reduced effectiveness of conventional therapies (Massagué and Obenauf, 2016).

Lung and bone niches

Among distant sites, the bone and lung represent the most frequent locations of breast cancer metastasis, with bone involvement occurring in approximately 70% of cases and lung involvement in around 30% (Buijs and van der Pluijm, 2009, Xiao et al., 2018). Each of these organs provides a distinct microenvironment that metastatic tumour cells must exploit and remodel in order to survive and proliferate (Schild et al., 2018).

The bone matrix, composed of rigid mineralised collagen and other extracellular components, is continuously remodelled by osteoclasts and osteoblasts, a process that metastatic cells hijack to create a supportive niche (Croucher et al., 2016, Kolb and Bussard, 2019). Breast cancer cells secrete parathyroid hormone-related protein (PTHrP), which stimulates osteoblasts to produce Receptor Activator of Nuclear factor-kB Ligand (RANKL), activating osteoclast-mediated bone resorption (Macedo et al., 2017). This

releases growth factors such as Transforming Growth Factor beta (TGF-β) from the bone matrix, further promoting tumour proliferation in a feed-forward “vicious cycle” of bone metastasis (Guise et al., 2006, Guise and Mundy, 1998, Paget, 1889). Tumour cells also respond to the rigid and hypoxic bone environment by activating mechanosignalling and stress-adaptive pathways, including TGF-β and GLI-Krupel family member 2 (GLI2) signalling, which enhance osteolytic activity and metastatic growth (Bolamperti et al., 2022, Page et al., 2015). This interplay between breast cancer cells and bone remodelling drives disease progression and contributes to the skeletal complications observed in patients (Chen et al., 2010).

In contrast to the rigid, hypoxic bone microenvironment, the lung presents a highly vascularised, oxygen-rich landscape that tumour cells capitalise on for metastatic colonisation (Altorki et al., 2019, Stevens et al., 2008). The dense capillary network in the lung facilitates early arrest of circulating breast cancer cells, enabling transendothelial migration into the parenchyma (Altorki et al., 2019, Stevens et al., 2008). Tumour-derived extracellular vesicles and soluble factors prime this niche by activating fibroblasts and endothelial cells to remodel the extracellular matrix and increase vascular permeability, thereby enhancing tumour cell seeding and survival (Medeiros and Allan, 2019). Additionally, breast cancer cells recruit bone marrow-derived myeloid cells and manipulate lung-resident immune populations, suppressing cytotoxic T-cell and natural killer (NK) cell activity to evade immune clearance (Giles et al., 2016, Medeiros and Allan, 2019, Xiang et al., 2009). Inflammatory cytokines such as tumour necrosis factor alpha (TNFα) amplify these stromal and immune alterations, reinforcing a pro-metastatic environment that supports sustained outgrowth (Chow et al., 2014, Hiratsuka et al., 2006). Together, these processes illustrate how breast cancer cells adapt to and reshape the lung microenvironment to support metastatic progression.

Understanding these organ-specific microenvironments is crucial, as their complex interplay with metastatic cancer cells governs disease progression, therapeutic resistance, and ultimately patient outcomes (de Visser and Joyce, 2023, Massagué and Obenauf, 2016). To study these organ-specific adaptations, researchers have developed lung metastatic (LM) and bone metastatic (BoM) sublines from the parental MDA-MB-231 triple-negative breast cancer cell line through organ-specific *in vivo* selection in immunodeficient mice (Kang et al., 2003, Minn et al., 2005). To generate BoM sublines, cancer cells were injected into the left cardiac ventricle, enabling systemic circulation and promoting the selection of clones with a propensity for bone colonisation (Kang et al., 2003). These BoM sublines overexpress genes such as C-X-C chemokine receptor type 4 (CXCR4) and interleukin-11 (IL-11), which facilitate bone remodelling, osteolysis, and tumour cell dormancy within the bone microenvironment (Kang et al., 2003, Sotiriou et al., 2001, Taichman et al., 2002). In contrast, LM sublines were established by injecting cells into the tail vein to selectively enrich variants with lung-tropic behaviour (Minn et al., 2005). These LM cells display elevated expression of genes including Matrix Metalloproteinase-1 (MMP1) and C-X-C motif chemokine ligand 1 (CXCL1), which promote angiogenesis, immune evasion, and adaptation to the lung niche (Minn et al., 2005, Balkwill, 2004, Egeblad and Werb, 2002). Together, these well-characterised sublines provide robust preclinical models that closely mirror the molecular specialisation and organotropism observed in breast cancer metastasis to the lung and bone, and they form the foundation for the investigations undertaken in this study.

Stress adaptations

During metastasis, cancer cells face multiple stresses as they detach from the primary tumour, travel through the circulation, and colonise distant organs (Fidler, 2003, Lambert et al., 2017). These include hypoxia, oxidative stress, and immune surveillance (Shen and

Kang, 2020). These hostile conditions trigger cancer cells to reprogramme multiple pathways, resulting in adaptations that are essential for survival and dissemination (Massagué and Obenauf, 2016). For example, hypoxia is common in solid tumours due to inadequate blood supply and triggers stabilisation of hypoxia-inducible factors, leading to changes in metabolism and promotion of invasive behaviours (Rankin et al., 2016). Reactive oxygen species (ROS) produced in response to oxidative stress modulate metabolic enzymes and signalling pathways, promoting tumour progression but requiring cancer cells to strengthen antioxidant defences to avoid lethal damage (Bhardwaj and He, 2020). In parallel, Immune surveillance by cytotoxic lymphocytes restricts metastasis, but metastatic cells evade destruction via antigen presentation alterations, immune checkpoint upregulation (such as PD-L1), and recruitment of immunosuppressive cells (Galassi et al., 2024). Metabolic rewiring and immune evasion are therefore key adaptations that allow metastatic cells to persist under these hostile conditions.

Alongside these, emerging evidence points to regulated cell death resistance as a central adaptation, equipping metastatic cells to survive stresses they encounter in the metastatic cascade, ultimately supporting successful colonisation (Peng et al., 2022, Su et al., 2015). Notably, recent attention has focused on non-apoptotic forms of regulated cell death, such as ferroptosis (Dixon et al., 2012, Peng et al., 2022).

Ferroptosis

Ferroptosis is a recently recognised, non-apoptotic form of regulated cell death, distinguished from apoptosis, necrosis, and autophagy by its unique cellular characteristics (Dixon et al., 2012). It is driven by iron-dependent lipid peroxidation and characterised morphologically by shrunken mitochondria with condensed membranes, reduced or absent cristae, and intact nuclei lacking chromatin condensation (Dixon et al., 2012).

At the biochemical level, ferroptosis results from an imbalance between lipid peroxide generation and antioxidant defence (Dixon et al., 2012). Polyunsaturated fatty acids (PUFAs) in membrane phospholipids are particularly susceptible to iron-dependent peroxidation via the Fenton reaction and lipoxygenase activity, leading to lethal lipid ROS accumulation (**Figure 1**) (Dixon et al., 2012). Normally, this is counteracted by the cystine/glutamate antiporter system X_c^-, in which the transporter subunit SLC7A11 mediates cystine import for glutathione (GSH) synthesis, and by glutathione peroxidase 4 (GPX4), which detoxifies lipid peroxides (**Figure 1**) (Dixon et al., 2012, Yang et al., 2014). Pharmacological blockade of SLC7A11 by compounds such as erastin, or its *in vivo* analogue imidazole ketone erastin (IKE), disrupts cystine uptake and depletes GSH, thereby sensitising cells to ferroptosis (Dixon et al., 2012, Larraufie et al., 2015). Conversely, ferroptosis can be suppressed by radical-trapping antioxidants such as ferrostatin-1 (Ferr-1), which inhibit lipid peroxidation and prevent the accumulation of toxic lipid ROS (Dixon et al., 2012).

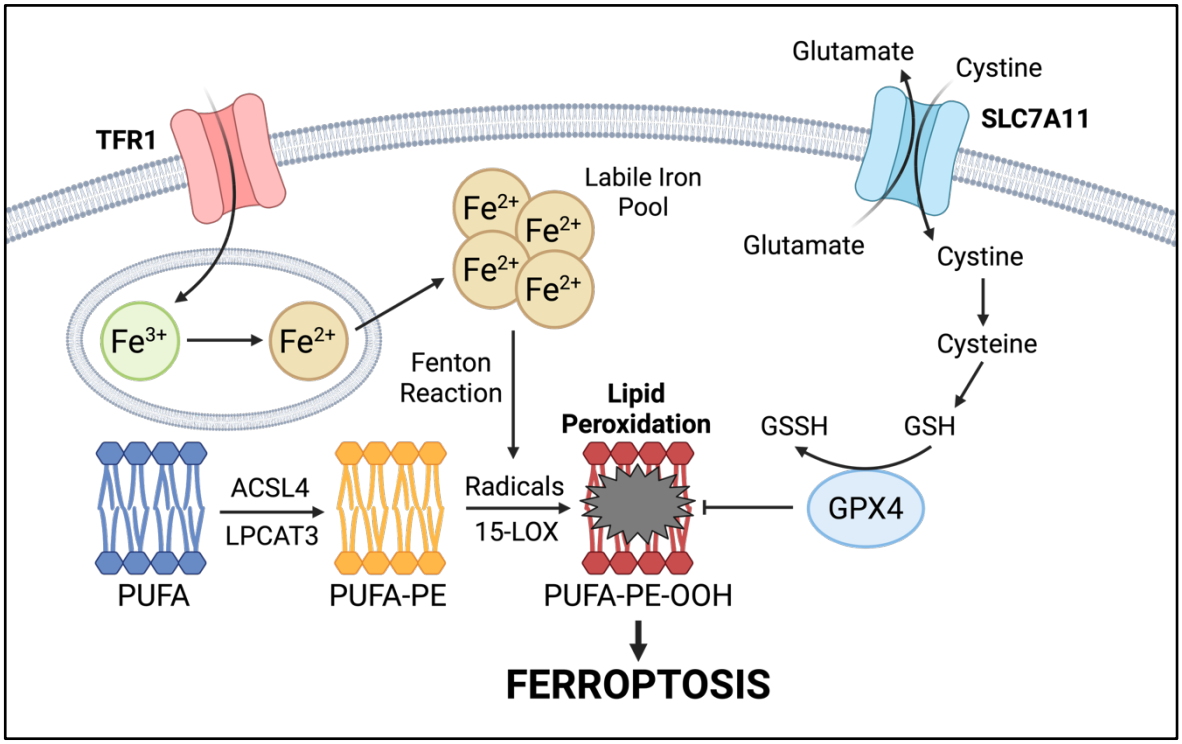


Figure 1: The ferroptosis pathway. *Iron is transported into the cell via TFR1, where Fe^{3+} is converted to Fe^{2+}, contributing to the labile iron pool. Fe^{2+} participates in the Fenton reaction, generating radicals that drive lipid peroxidation. PUFA in the membrane is converted to PUFA-PE through the action of ACSL4 and LPCAT3. PUFA-PE undergoes oxidation via 15-LOX, forming PUFA-PE-OOH. Accumulation of these oxidised phospholipids triggers ferroptosis. SLC7A11 imports cystine in exchange for glutamate; cystine is reduced to cysteine, which is required for GSH synthesis. GSH acts as a substrate for GPX4, which reduces PUFA-PE-OOH and prevents lipid peroxidation and ferroptosis. Inhibition or depletion of SLC7A11, GSH, or GPX4 leads to PUFA-PE-OOH accumulation and ferroptosis. TFR1, transferrin receptor 1; PUFA, polyunsaturated fatty acid; ACSL4, acyl-CoA synthetase long-chain family member 4; LPCAT3, lysophosphatidylcholine acyltransferase 3; PE, phosphatidylethanolamine; 15-LOX, 15-lipoxygenase; GSH, glutathione; GSSH, glutathione disulfide; GPX4, glutathione peroxidase 4. Figure generated using BioRender.*

Ferroptosis is increasingly implicated in cancer biology. Tumour cells can evade ferroptotic stress through upregulation of antioxidant pathways (e.g., SLC7A11, GPX4), enabling survival in hostile microenvironments (Dixon et al., 2012, Viswanathan et al., 2017, Yang et al., 2014). For example, melanoma cells in circulation experience ferroptotic pressure due

to plasma iron and ROS, whereas the lymphatic niche provides protection via glutathione availability and other antioxidant mechanisms (Ubellacker et al., 2020). Similarly, transcriptional regulators such as sterol regulatory element binding protein 2 (SREBP2) and 2,4-dienoyl-CoA reductase 1 (DECR1) promote lipid metabolism adaptations that protect metastatic cells from ferroptosis and support invasive behaviour (Hong et al., 2021, Nassar et al., 2020).

Although ferroptosis has been implicated in tumour progression and metastasis across several cancers, its role in breast cancer is not fully understood (Zhang et al., 2023). Metastatic breast cancer cells may exhibit altered ferroptotic sensitivity, representing a potential vulnerability that could be therapeutically exploited. Moreover, the ways in which ferroptosis intersects with anti-tumour immune responses remain poorly understood, highlighting an important gap in our understanding of metastatic disease.

Antigen presentation

Antigen presentation via MHC class I (MHC-I) molecules enables cytotoxic $CD8^+$ T cells to detect and eliminate tumour cells by displaying intracellular peptides, including tumour-derived antigens (Yang et al., 2023). Downregulation of MHC-I is a common strategy by which metastatic cancer cells evade immune surveillance, promoting survival in distant organs such as bone and lung (Dhatchinamoorthy et al., 2021). Suppression of antigen presentation is therefore a critical adaptation during metastatic progression, allowing tumour cells to persist despite active immune surveillance (Dhatchinamoorthy et al., 2021). In metastatic breast cancer, evidence suggests that antigen presentation pathways are frequently impaired (Pedersen et al., 2017), which may not only facilitate immune evasion but also interact with other stress-response mechanisms such as ferroptosis, underscoring the need to understand how these pathways are coordinated.

Recent studies indicate a complex interplay between ferroptosis and the immune response. Early ferroptotic tumour cells can promote anti-tumour immune responses via immunogenic cell death (ICD), including the release of damage associated molecular patterns (DAMPs), which can activate dendritic cells and modulate tumour antigenicity (Gong et al., 2020, Demuynck et al., 2021). Conversely, ferroptotic stress in the tumour microenvironment can impair $CD8^+$ T cell and NK cell function by inducing lipid peroxidation, inhibiting proliferation, and reducing cytotoxic activity (Ma et al., 2021, Poznanski et al., 2021). Early ferroptotic cancer cells have also been shown to inhibit dendritic cell maturation and antigen cross-presentation, thereby dampening adaptive immune responses (Wiernicki et al., 2022). This dual role highlights the importance of understanding how metastatic tumour cells manipulate both stress and immune pathways.

Despite growing interest in ferroptosis and its interactions with the immune system, it remains unclear whether and how ferroptotic stress influences antigen presentation in metastatic breast cancer. In particular, the effects of ferroptosis on MHC-I expression and subsequent immune recognition have not been defined. Understanding this relationship is critical, as it may reveal mechanisms of immune evasion in metastasis and identify opportunities to manipulate ferroptosis to enhance anti-tumour immunity.

Study aims

The overarching goal of this study is to investigate the role of ferroptosis in breast cancer metastasis, specifically lung and bone, and to identify potential vulnerabilities in these metastatic cells that could inform the development of more effective therapies. Specifically, we aim to:

1. Identify molecular characteristics in metastatic breast cancer cells, focusing on antigen presentation and ferroptosis defence pathways.
2. Determine whether metastatic breast cancer cells exhibit altered ferroptosis sensitivity.

3. Assess whether ferroptosis induction modulates MHC-I expression in metastatic breast cancer cells.

Materials and Methods

Tissue Culture

MDA-MB-231 WT (wild-type) (ATCC), LM (lung metastatic), and BoM (bone metastatic) cells were cultured in Dulbecco's Modified Eagle Medium (DMEM; Gibco, 41966-029) supplemented with 10% heat-inactivated foetal bovine serum (FBS; Sigma, F7524) and 1% antibiotic–antimycotic (anti–anti; Sigma, A5955). The LM and BoM sublines were kindly provided by Massagué group, and are metastatic derivatives of the parental line, established through *in vivo* selection in immunocompromised mice (Kang et al., 2003, Minn et al., 2005). Jurkat 1G4 cells (BPS Bioscience, 78769), engineered to express the human NY-ESO-1-specific T-cell receptor clone 1G4 and an NFAT-driven GFP reporter, were kindly provided by Dr Ahmet Hazini and maintained in RPMI 1640 supplemented with 10% FBS, 1% anti–anti, 1% L-glutamine (Gibco, 25030081), and 1% sodium pyruvate. All cell lines were maintained at 37 °C in a humidified incubator with 5% CO_2 and routinely tested for mycoplasma contamination. Cells were passaged using 0.05% trypsin–EDTA (Sigma, T3924).

Reagents

Erastin (APExBIO, B1524) was dissolved in Dimethyl sulfoxide (DMSO) at 5 mM stock concentration, Ferrostatin-1 (Ferr-1; Abcam, ab146169-5mg) was dissolved in DMSO at 10 mM stock concentration, FerroOrange (Dojindo, F374) was dissolved in DMSO at 1 mmol/l stock concentration, and NY-ESO-1 peptide (IBA Lifesciences, 15352126), kindly provided by Dr. Ahmet Hazini, was dissolved in DMSO at 1 mM stock concentration. All reagents were diluted in cell culture media to specified concentrations.

T Cell Activation Assay

Jurkat 1G4 cells, engineered to express the NY-ESO-1-specific T-cell receptor clone 1G4 and an NFAT-driven GFP reporter, were used to assess antigen-specific T-cell activation. MDA-MB-231 WT, LM, or BoM cells were seeded at 2 x 10^4 cells per well in 96-well plates. Jurkat 1G4 cells were added at 4 x 10^4 cells per well, together with NY-ESO-1 peptide at a final concentration of 2.5 µM. Co-cultures were incubated for 20 hours at 37 °C. Jurkat T-cell activation was measured by quantifying GFP expression using the Celigo imaging cytometer (Nexcelom). Jurkat 1G4 cells and NY-ESO-1 were kindly provided by Dr. Ahmet Hazini.

Cell Viability Assay

Cell viability was assessed using the CellTiter-Blue Cell Viability Assay (Promega). MDA-MB-231 WT, LM, and BoM cells were seeded at a density of 5 x 10^3 cells per well in 96-well plates. After 24 hours of incubation at 37 °C, cells were treated with a range of Erastin concentrations (10, 5, 2, 1, 0.5, and 0 µM), with DMSO used as a vehicle control. Cells were also co-treated with either 2 µM Ferr-1 or DMSO. Following treatment and incubation for 24 hours, media were removed, and cells were washed once with phosphate-buffered saline (PBS; Oxoid, BR0014G). CellTiter-Blue reagent, diluted 1:5 in PBS as per manufacturer's instructions, was added directly to each well, and plates were incubated at 37 °C for 1 hour. Fluorescence (excitation: 560 nm, emission: 590 nm) was directly imaged following incubation using a BMG Labtech POLARstar Omega plate reader.

FerroOrange Assay

MDA-MB-231 WT, LM, and BoM cells were seeded at 5 x 10^3 cells per well in 96-well plates. After 18 hours of incubation at 37 °C, ammonium iron (II) sulfate was added to designated positive control wells. After 24 hours from initial seeding, cells were washed with PBS and incubated with 1 µmol/L FerroOrange solution in serum-free phenol red-free media (Gibco, 31053028) for 30 minutes at 37 °C, protected from light. Fluorescence (excitation: 543 nm, emission: 580 nm) was directly imaged following incubation using the Celigo imaging cytometer.

Immunofluorescence Staining

MDA-MB-231 WT, LM, and BoM cells were seeded at 2.5 x 10^5 cells per well in 6-well plates containing sterile glass coverslips and incubated for 24 hours at 37 °C.

Cells were washed once with PBS before fixation with 4% PFA for 10 minutes at room temperature. After fixation, cells were washed with PBS and permeabilised with 0.1% Triton X-100 (Sigma, H5141) in PBS for 10 minutes at room temperature. Cells were washed again with PBS and then blocked with 1% BSA and 0.1% Tween-20 in PBS for 1 hour at room temperature. Primary antibody against HLA-ABC (Abcam, ab70328), diluted 1:500 in 1% BSA and 0.1% Tween-20 in PBS, was applied overnight at 4 °C in a humidified environment. Following primary incubation, cells were washed with PBS and incubated with anti-mouse Alexa Fluor 647 secondary antibody (Invitrogen, A21237), diluted 1:250 in 1% BSA and 0.1% Tween-20 in PBS, for 1 hour at room temperature protected from light. Nuclei were counterstained with DAPI for 30 minutes. Coverslips were mounted using Fluoromount mounting medium (Sigma, F4680-25ML). Images were acquired using a Zeiss Airyscan 880 confocal microscope.

Flow Cytometry

Live Cell Staining for Lipid Peroxidation and Lipid Droplets

To assess lipid peroxidation and lipid droplet accumulation, MDA-MB-231 WT, LM, and BoM cells were seeded at 8.5×10^4 cells per well in 12-well plates. Cells were incubated for 24 hours prior to treatment. Cells were then treated with either 2.5 µM erastin or DMSO and incubated for an additional 24 hours. Cell culture medium was then removed and replaced with staining solution consisting of either 1 µM BODIPY™ 581/591 C11 (ThermoFisher, D3861) or 1 µg/mL BODIPY™ 493/503 lipid droplet stain (ThermoFisher, D3922), diluted in PBS. Staining was performed for 30 minutes at 37 °C, protected from light. An unstained control was also included per cell line. Following staining, cells were washed with PBS, trypsinised, and collected in medium. Samples were centrifuged at 400 × g for 5 minutes, supernatant discarded, and pellets resuspended in FACS buffer (PBS containing 2% FBS and 0.5 mM EDTA (Invitrogen, 15575020)). Cells were transferred to a U-bottom 96-well plate and kept on ice until analysis. Flow cytometry analysis was performed on a CytoFLEX (Beckman Coulter), with BODIPY probes detected in the FITC channel.

Antibody-Based Cell Surface Staining

To assess HLA surface expression, 1×10^5 MDA-MB-231 WT, LM, or BoM cells were seeded per well in 6-well plates. After 24 hours, cells were treated with either 2.5 µM erastin or DMSO. Following another 24-hour incubation, cells were washed with PBS and centrifuged at 400 × g for 5 minutes. Cell pellets were resuspended in antibody staining solution prepared in FACS buffer and incubated for 30 minutes at 4 °C in the dark. See **Table 1** for antibody dilutions. Unstained controls were resuspended in FACS buffer only. Stained cells were then washed with PBS, centrifuged at 400 × g for 5 minutes, and resuspended in FACS buffer before being transferred to a U-bottom 96-well plate. Samples

were analysed using the CytoFLEX, with fluorophores detected in the appropriate channels (**Table 1**).

Table 1. Antibodies used for surface HLA staining

Antibody	Fluorophore	Supplier (Catalogue No.)	Dilution
HLA-ABC	Pacific Blue	BioLegend, 311418	1:300
HLA-A2	PE	BioLegend, 343305	1:200

Western Blotting

Protein Extraction and Quantification

Cells were washed once with cold PBS and centrifuged at 400 × g for five minutes at 4 °C. The resulting pellet was lysed in 1× RIPA lysis buffer (EMD Millipore, 3519190, supplemented with phosphatase (PhosSTOP; Roche, 04906837001) and protease inhibitors (Complete EASYpack; Roche, 0493116001). Lysates were sonicated for 10 seconds and centrifuged at maximum speed (17,000 x g) for up to 10 minutes at 4 °C. The supernatant was collected for downstream analysis. Protein concentration was quantified using the Pierce™ BCA Protein Assay Kit (Thermo, 23225), following the manufacturer's instructions.

Sample Preparation and Gel Electrophoresis

For sample preparation, 40 µg of total protein was diluted in 4× LDS Sample Buffer (Novex Bolt, B0007) and 10× Sample Reducing Agent (Novex Bolt, B0009), boiled at 95 °C for five minutes, and loaded onto 4–12% Bis-Tris gels (Invitrogen, NW04120BOX). Gels were run using MES SDS Running Buffer (Invitrogen, B0002). A pre-stained molecular weight ladder (Biorad Kaleidoscope) was included for size estimation.

Protein Transfer and Blocking

Proteins were transferred onto PVDF membranes (Biorad, #10026933) using the Biorad Trans-Blot Turbo Transfer System and transfer stacks (L00244B) with transfer buffer (Biorad, #10026938). Membranes were blocked for 1 hour at room temperature in 5% BSA (Sigma-Aldrich, A7030-100G) in tris buffer saline with 0.1% Tween-20 (TBST).

Antibody Incubation and Detection

Membranes were incubated overnight at 4 °C with primary antibodies diluted 1:1000 in 5% BSA in TBST containing sodium azide (NaN_3; Sigma, 18101-023). The primary antibodies used are detailed in **Table 2**. Following incubation, membranes were washed in TBST. Secondary antibodies (**Table 2**) were diluted 1:5000 in 5% BSA in TBST and incubated with membranes for 1 hour at room temperature. After incubation, membranes were washed again in TBST. Signal detection was performed using Biorad Clarity Western ECL substrates (10203181, 10203837) and visualised by chemiluminescence imaging.

Table 2. Antibodies Used

Antibody	Host Species	Supplier & Catalogue Number
Primary Antibodies		
SLC7A11	Rabbit	Cell Signaling (D2M7A)
HLA ABC	Mouse	Abcam (ab70328)
GPX4	Mouse	R&D Systems (MAB5457)
Transferrin	Rabbit	Cell Signaling (E7F4T)
Secondary Antibodies		

Anti-mouse	Rabbit	Cell Signaling (Lot 38)
Anti-rabbit	Goat	Jackson ImmunoResearch (711-035-152)

In vivo Studies

All *in vivo* experiments were conducted according to the guidelines of the United Kingdom Home Office and the University of Oxford under the project license PP4558762. Female NOD.Cg-Prkdc^{scid} Il2rg^{tm1Wjl}/SzJ (NSG) mice were purchased from Charles River (6 - 8 weeks) and housed in individually ventilated cages containing no more than six mice per cage, in a 12/12-hour light/dark cycle. Mice were monitored regularly for health, weight, and tumour burden throughout the duration of the studies.

For *in vivo* tumour studies, mice were orthotopically injected in the mammary fat pad with 1 × 10^6 MDA-MB-231 WT, LM, or BoM sublines (n = 6 per group). Cells prepared in FBS free media:Matrigel (Corning, 354230) in 1:1 ratio. For the IKE treatment study, once tumours reached ~50 mm³, mice were randomised into two groups (n = 3 per treatment group) to receive either 50 mg/kg IKE (Selleckchem, S8877) or vehicle control (5 % DMSO, Sigma-Aldrich, D2650) intraperitoneally three times weekly. IKE was dissolved in HBSS and pH-adjusted to 4.

Mice were humanely culled at experimental endpoints defined by tumour volume reaching 1,000 mm³. Primary tumours, lungs, and hind leg bones (where applicable) were collected for analysis. Tumour samples were fixed in 10% formalin for 24 hours prior to transfer to 70% ethanol. Lung tissues were inflated with formalin before fixation, and bone samples were decalcified with 14% EDTA (Sigma, E5134) at pH 7.2 for six weeks following fixation.

Immunohistochemistry (IHC)

Processing, Embedding, and Sectioning

Fixed tissue samples were processed overnight using a Thermo Scientific STP120 tissue processor and subsequently embedded in paraffin wax (Histoplast PE, Thermo Scientific, 8330). Paraffin-embedded tissues were sectioned at 6 µm thickness using a Bright 7010 microtome with MX35 Premier blades. Sections were mounted onto Superfrost Plus adhesion microscope slides (Epredia, 10149870).

Deparaffinisation and Rehydration

Slides were incubated briefly at 60 °C, then deparaffinised by two rounds of Citroclear (Histo-Clear, National Diagnostics). This was followed by sequential washes in 100%, 95%, 70%, and 50% ethanol, before rinsing in distilled water.

Antigen Retrieval and Blocking

Antigen retrieval was performed using 1x citrate buffer (pH 6.0) (Sigma-Aldrich, C9999), diluted with deionized water and 0.05 % Tween-20, in a Biocare Medical Decloaking Chamber at 110 °C for three minutes. Slides were cooled down at room temperature for 20 mins. Endogenous peroxidase activity was blocked with blocking solution (BLOXALL, Vector, SP-6000-100) and incubated for 20 minutes. Slides were then washed in PBS with 0.05 % Tween-20 (PBST). Non-specific binding was blocked by incubating slides with normal goat serum (SeraCare KPI, 5560-0007) at room temperature for 20 minutes.

Primary and Secondary Antibody Incubations

Primary antibodies (**Table 3**) were diluted in antibody diluent (Abcam, AB64211) and incubated overnight at 4 °C. After primary antibody incubation, slides were washed with

PBST. Secondary antibodies (Dako Anti-Rabbit K4003 or Anti-Mouse K4001) were applied and incubated at room temperature for 20 minutes. Slides were again washed with PBST.

Table 3. Primary IHC Antibodies

Antibody	Host Species	Supplier & Catalogue Number	Dilution
4HNE	Rabbit	bs-6313R	1:100
HLA-ABC	Mouse	Abcam (ab70328)	1:10,000
Ki67	Rabbit	Abcam (ab16667)	1:200

Detection and Counterstaining

Detection was performed using Dako (Diaminobenzidine) DAB chromogen (K3468). DAB incubation time was determined empirically based on tissue type. Slides were counterstained with haematoxylin (Sigma, GHS132) diluted 1:5 in ddH_2O. After counterstaining, slides were mounted with an aqueous mounting medium (Aquatex, Sigma, 108562).

Iron Staining

Following deparaffinisation and rehydration as previously described, slides were incubated with a 1:1 solution of potassium ferrocyanide (Abcam, ab73331) and hydrochloric acid (Abcam, ab73330) for one hour in the dark.

An optimisation step was performed where slides were washed with ddH_2O and incubated in a freshly prepared solution containing methanol (Sigma-Aldrich, 34860), 0.3 M sodium azide (NaN_3; Sigma-Aldrich, 18101-023), and 9.8 M hydrogen peroxide (H_2O_2; Sigma-Aldrich, 31642). Slides were then washed with PBS before proceeding to DAB staining using Dako DAB chromogen (K3468). DAB incubation time was determined empirically based on tissue type.

After iron staining and optimisation, slides were counterstained with nuclear fast red (Abcam, ab74102) for three minutes, rinsed in running tap water, then dehydrated through 50%, 70%, 95%, and 100% ethanol, followed by two rounds of xylene. Slides were mounted using DPX mountant (Sigma-Aldrich, 06522).

Bone Tissue Microarray

Iron staining was performed on a human bone tissue microarray (TMA) slide (Biomax, BO801), which contains cores from patient-derived normal and cancerous bone tissue. The TMA was incubated at 60 °C for 1 hour prior to staining. Slides were deparaffinised and rehydrated following the same protocol as described above. Iron staining was then performed as outlined in the *Iron Staining* section. Only bone tissue regions were included in the quantification, with adipose tissue excluded from the analysis.

IHC analysis

Whole slide images of stained tissue sections were acquired and analysed using a combination of QuPath and ImageJ. In QuPath, tissue folds were excluded from the scans prior to analysis. Ki67 staining was quantified by selecting three representative regions of interest (ROIs; 10× magnification) per tissue section, and positive cells were quantified using QuPath's cell classification tool.

Iron staining was assessed in ImageJ, where brown iron-positive signal was isolated by splitting RGB channels and applying fixed thresholds across all samples within the same experiment. Particle analysis was performed to measure integrated intensity of the brown channel. The percentage area positive for iron was then calculated as a readout of iron deposition.

All other staining was quantified in ImageJ by isolating DAB signal through colour deconvolution. Brightness/contrast (minimum and maximum values) was adjusted

uniformly across samples within the same experiment, and integrated intensity of the DAB channel was measured as a readout of marker expression.

RNA-Sequencing Analysis

RNA-sequencing data comparing MDA-MB-231 LM and BoM metastatic sublines to the parental MDA-MB-231 (WT) cells were previously generated by our laboratory. Differential gene expression analysis was performed to identify genes consistently downregulated in both metastatic sublines relative to WT. Gene lists and associated fold changes for LM versus WT and BoM versus WT comparisons were compiled and used for downstream analysis. Pathway enrichment analysis was carried out using the Database for Annotation, Visualization, and Integrated Discovery (DAVID) clustering tool to identify significantly affected biological pathways (Huang et al., 2009). Pathways of interest, including antigen presentation and ferroptosis defence, were selected for closer examination to investigate mechanisms relevant to immune recognition and ferroptotic stress. Enrichment plots were subsequently generated using the SRplot tool to visualise the pathway enrichment results (Tang et al., 2023).

Statistical Analysis

Statistical analyses were performed using GraphPad Prism software (GraphPad Prism 10, Dotmatics). Data are presented as the mean ± standard deviation (SD), unless otherwise indicated. The specific statistical tests applied varied depending on the experiment and are described in the relevant figure legends. A p-value of less than 0.05 was considered statistically significant.

Results

Suppressed ferroptosis defence and antigen presentation in metastasis

Molecular characterisation was performed on metastatic breast cancer models to assess differences between parental (WT) MDA-MB-231 cells and their lung (LM) and bone (BoM) metastatic sublines, integrating gene set enrichment analysis, protein quantification, and functional analyses in matched *in vitro* cell lines.

A previously generated RNA sequencing dataset from our laboratory, comparing LM and BoM breast cancer sublines to WT MDA-MB-231 cells, was used to analyse global changes in gene expression. Genes exhibiting reduced expression in both LM versus WT and BoM versus WT comparisons were selected, and functional clustering was performed using the Database for Annotation, Visualization, and Integrated Discovery (DAVID) (Huang et al., 2009). Consistently suppressed pathways were visualised in an enrichment plot, which displays enrichment scores along with statistical significance, highlighting the biological processes most impacted in metastatic cells (**Figure 2A**). Among these, antigen presentation pathways and ferroptosis defence were notably downregulated (**Figure 2A**). To illustrate the contribution of each metastatic subline individually, separate enrichment plots for LM versus WT and BoM versus WT are provided in **Appendix A**, showing similar patterns of downregulation for these pathways. Antigen presentation is crucial for effective immune recognition, as it enables tumour cells to display peptides to cytotoxic T cells, facilitating immune-mediated tumour clearance (Yang et al., 2023, Dhatchinamoorthy et al., 2021). Ferroptosis defence involves cellular mechanisms that protect against iron-dependent lipid peroxidation and regulated cell death, a vulnerability that cancer cells may exploit to survive in hostile metastatic environments (Dixon et al., 2012, Lei et al., 2022a). The observed suppression of these pathways suggests metastatic sublines may evade immune surveillance and ferroptotic cell death, contributing to metastatic progression.

To validate these transcriptomic findings at the protein level, western blotting was performed for MHC-I, SLC7A11, GPX4, and Transferrin. MHC-I, an essential molecule for antigen presentation to cytotoxic T cells, was substantially decreased in LM and BoM cells compared with WT, indicating impaired antigen presentation machinery (**Figure 2B**). The ferroptosis suppressor SLC7A11 was markedly reduced in both LM and BoM sublines, whereas GPX4, another ferroptosis suppressor, showed a slight reduction in BoM and a more pronounced decrease in LM, consistent with attenuated ferroptosis defence. Transferrin, an iron transporter involved in ferroptosis regulation through iron availability, remained consistent across sublines (**Figure 2B**)

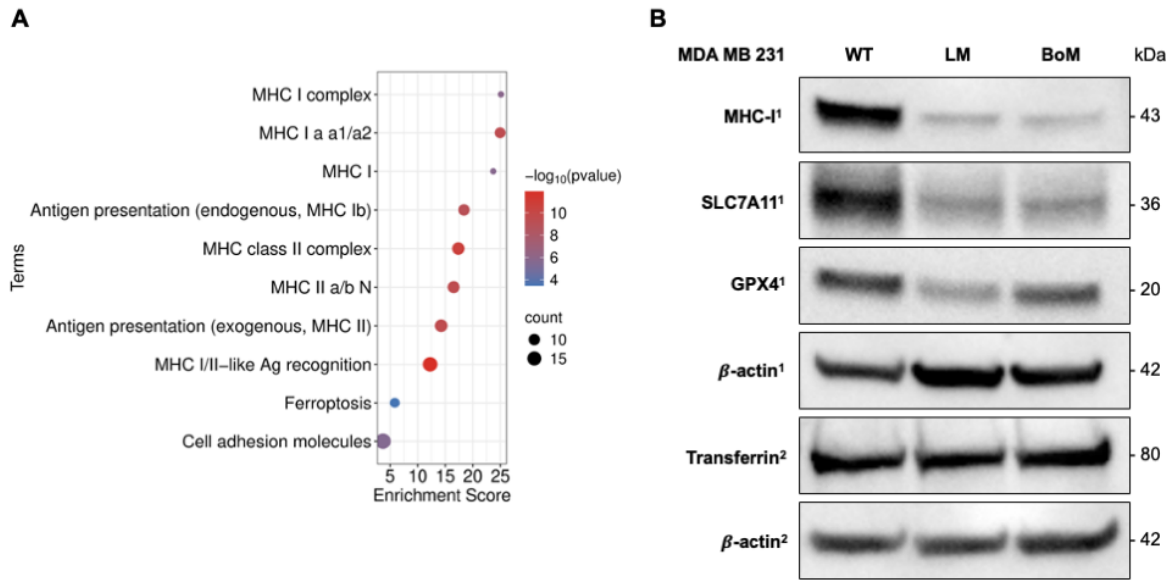


Figure 2: Downregulation of antigen presentation and ferroptosis defence pathways in lung and bone metastatic sublines confirmed by transcriptomic enrichment and protein analyses. ***A:*** *DAVID enrichment analysis of genes consistently downregulated in MDA-MB-231 LM and BoM metastatic sublines compared to WT cells. Enriched pathways include antigen presentation and ferroptosis defence, selected for closer examination in line with our study aims, and highlight intrinsic differences between metastatic and parental sublines.* ***B:*** *Western blot analysis of MHC-I, SLC7A11, GPX4, and Transferrin protein expression in MDA-MB-231 WT, LM, and BoM sublines. MHC-I and the ferroptosis suppressors SLC7A11 and GPX4 are reduced in LM and BoM compared with WT, with GPX4 showing a slight reduction in BoM and a more pronounced decrease in LM. The iron transporter Transferrin remains consistent across sublines.*

β-actin was used as a loading control for each membrane. Superscripts ¹, ² indicate that proteins were detected on separate blots.

To further visualise MHC-I surface expression, we performed immunofluorescence staining on WT, LM, and BoM cells, followed by confocal microscopy and quantitative image analysis (CellProfiler). Metastatic cells exhibited significantly lower MHC-I surface staining intensity than WT cells (**Figure 3A**), confirming protein-level downregulation observed by western blot.

To determine whether this reduction in MHC-I levels translated into functional impairment and affected antigen-specific T cell activation, WT, LM, and BoM cells were co-cultured with Jurkat 1G4 reporter T cells in the presence of NY-ESO-1 peptide for 20 hours. In this assay, cancer cells present the NY-ESO-1 peptide via HLA-A2, and GFP expression in the Jurkat cells serves as a readout of antigen-specific T cell activation. Jurkat activation was significantly reduced in BoM cells compared to WT, while LM cells showed a trend towards lower activation that did not reach statistical significance (**Figure 3B**). These results

demonstrate that decreased MHC-I expression in metastatic sublines, particularly BoM, impairs their capacity to activate antigen-specific T cells.

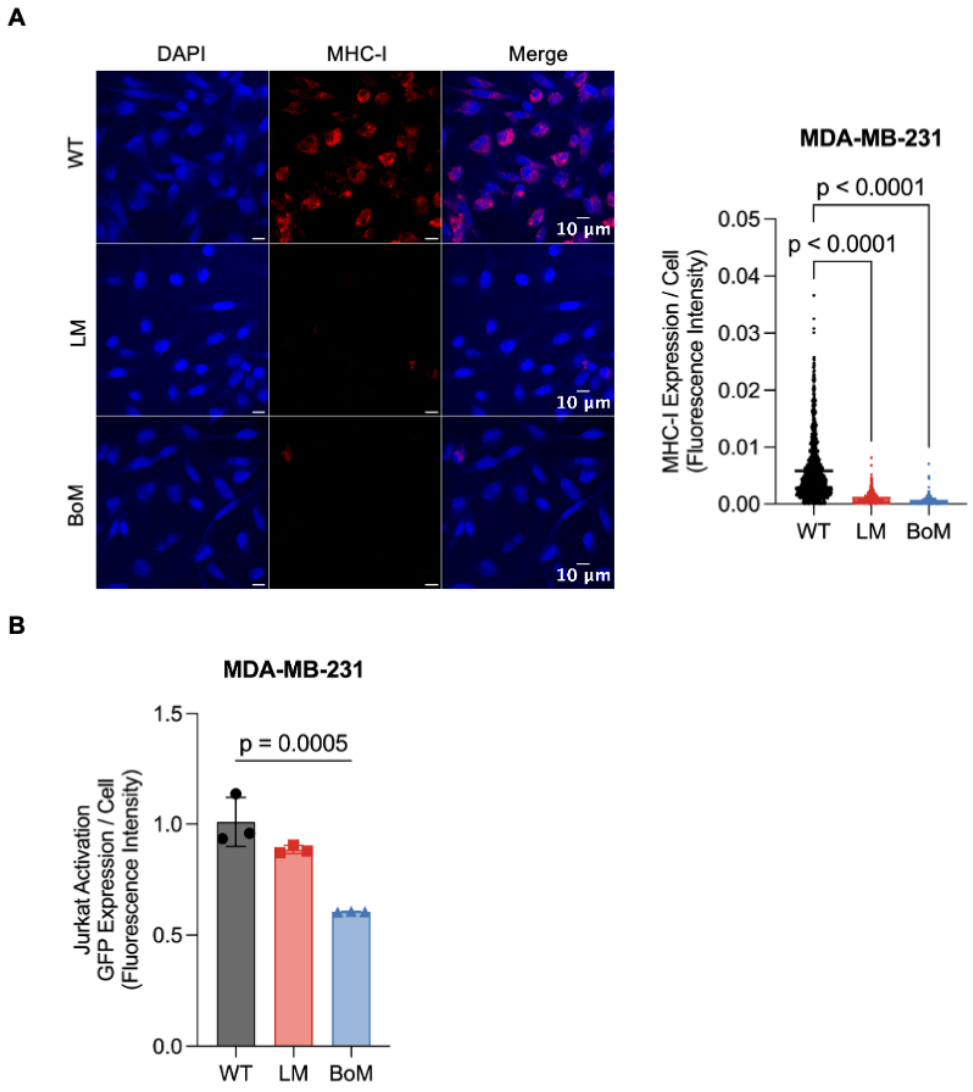


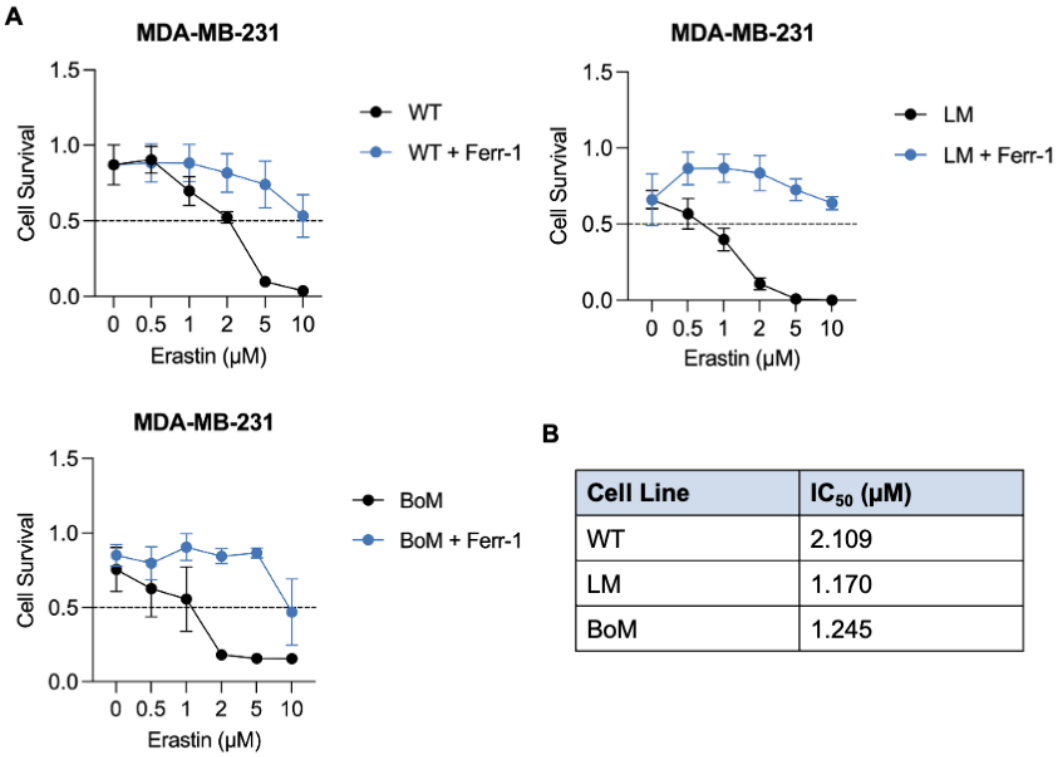
Figure 3: Reduced MHC-I surface expression in metastatic cells results in impaired T cell activation. A: *Representative immunofluorescence images of MDA-MB-231 WT, LM, and BoM sublines, showing DAPI (blue), MHC-I (far red), and merged channels (right). Quantification of MHC-I fluorescence intensity per cell was performed using CellProfiler from ten randomly selected fields of view per subline. Both LM and BoM cells show significantly reduced MHC-I expression compared to WT. Statistical analysis by Kruskal-Wallis test with Dunn's multiple comparisons revealed a significant difference between groups ($p < 0.0001$). Dunn's test confirmed significant reductions for WT vs. LM (adjusted $p < 0.0001$) and WT vs. BoM (adjusted $P < 0.0001$). Scale bars represent 10 µm.* ***B:*** *Jurkat 1G4 T cell activation measured as GFP fluorescence intensity per cell following 20-*

hour co-culture with WT, LM, or BoM cells in the presence of NY-ESO-1 peptide. Data from three technical replicates show a significant reduction in T cell activation in BoM compared to WT (ordinary one-way ANOVA, p = 0.0007; Dunnett's multiple comparisons: WT vs. BoM, adjusted p = 0.0005), while the reduction observed in LM did not reach statistical significance (adjusted p = 0.0964).Jurkat 1G4 T cells and NY-ESO-1 were kindly provided by Dr. Ahmet Hazini.

Metastatic cells exhibit increased sensitivity to ferroptosis

To investigate whether metastatic tumour cells exhibit increased sensitivity to ferroptosis, we performed analyses comparing WT MDA-MB-231 breast cancer cells with their LM and BoM metastatic sublines. This included *in vitro* assays measuring cell survival and lipid peroxidation, quantification and imaging of intracellular iron levels, and histological examinations of patient bone TMAs for iron staining.

To examine ferroptosis sensitivity in metastatic cells, we assessed cell survival of WT, LM, and BoM sublines treated with increasing concentrations of erastin, a ferroptosis inducer (SLC7A11 inhibitor), in the presence or absence of the ferroptosis inhibitor ferrostatin-1 (Ferr-1). Cell survival was measured using the CellTiter Blue assay and decreased to a greater extent in LM and BoM compared to WT, indicating enhanced ferroptosis sensitivity (**Figure 4A**). Ferr-1 rescued survival in all cell lines, confirming that cell death was ferroptosis dependent. IC_{50} values for erastin were calculated from survival curves, revealing lower IC_{50} for LM and BoM (1.170 μM and 1.245 μM respectively) compared to WT (2.109 μM) (**Figure 4B**). These data indicate that metastatic sublines exhibit increased susceptibility to erastin-induced ferroptosis relative to WT cells.



Cell Line	IC_{50} (μM)
WT	2.109
LM	1.170
BoM	1.245

Figure 4: Increased ferroptosis sensitivity in metastatic cells revealed by decreased survival and lowered IC_{50}. A: *Cell survival of WT, LM, and BoM sublines treated with increasing concentrations of erastin, with or without Ferr-1. Survival was measured after 24 hours using the CellTiter Blue assay. Data points represent mean ± SD from four technical replicates. Ferr-1 partially rescues cell survival, confirming ferroptosis-dependent cell death.* ***B:*** *Table summarising calculated IC_{50} values for erastin in WT, LM, and BoM cells derived from the dose-response curves (A). Representative graphs from multiple independent experiments are shown.*

Lipid peroxidation, a hallmark of ferroptosis, was assessed in WT, LM, and BoM cells treated with 2.5 μM erastin or vehicle control using the BODIPY™ 581/591 C11 probe and flow cytometry. Erastin treatment increased lipid peroxidation in all sublines compared to their respective controls, with the fold change being greater in LM and BoM cells than in WT cells (**Figure 5A-C**). These results align with enhanced ferroptosis sensitivity observed in metastatic sublines (**Figure 4**).

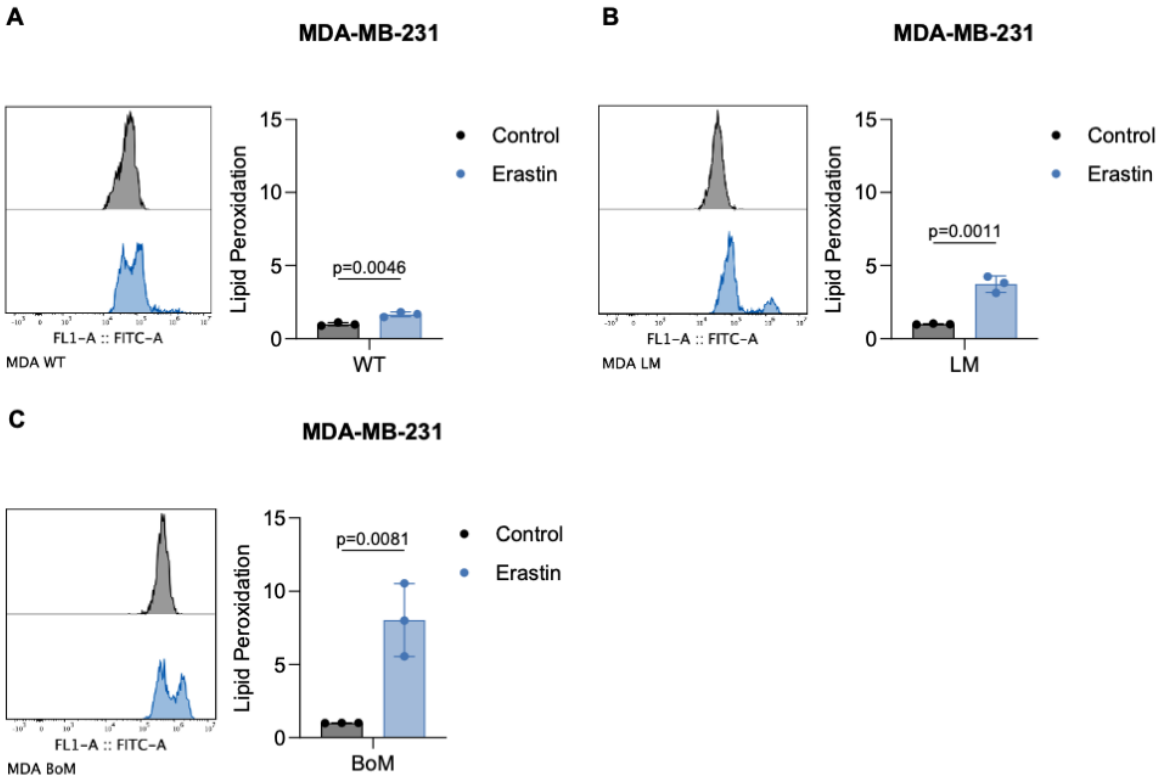


Figure 5: Erastin treatment increases lipid peroxidation in MDA-MB-231 sublines. *Flow cytometric analysis of lipid peroxidation in (**A**) WT, (**B**) LM, and (**C**) BoM sublines treated with 2.5 μM erastin or vehicle control. Left panels show representative histogram overlays of control (grey) and erastin-treated (blue) cells. Right panels show quantification of lipid peroxidation using the fluorescent probe BODIPY-C11 detected in the FITC channel, normalised to unstained controls. Data represent the fold change in geometric mean FITC fluorescence relative to vehicle control for each subline, from three technical replicates. Error bars indicate standard deviation. Statistical significance between control and erastin treatment was determined by unpaired t-tests, with p-values indicated above the bars.*

As ferroptosis is dependent on iron levels, we measured intracellular iron using the iron-specific fluorescent dye FerroOrange in MDA-MB-231 WT, LM, and BoM cells. Both LM and BoM metastatic sublines displayed higher intracellular iron than WT cells, with BoM cells exhibiting the greatest accumulation (**Figure 6A**).

Given the pronounced iron accumulation in BoM cells, we next examined histological iron staining in patient bone tumour tissue microarrays containing various malignant bone and cartilage tumours and their normal adjacent tissue (NAT). Malignant bone tumours exhibited markedly higher iron levels compared to NAT, suggesting that increased iron accumulation may be associated with malignant bone pathology (**Figure 6B**).

These data indicate that metastatic breast cancer cells, particularly those colonising bone, tend to accumulate elevated intracellular iron, which could be associated with altered ferroptosis sensitivity.

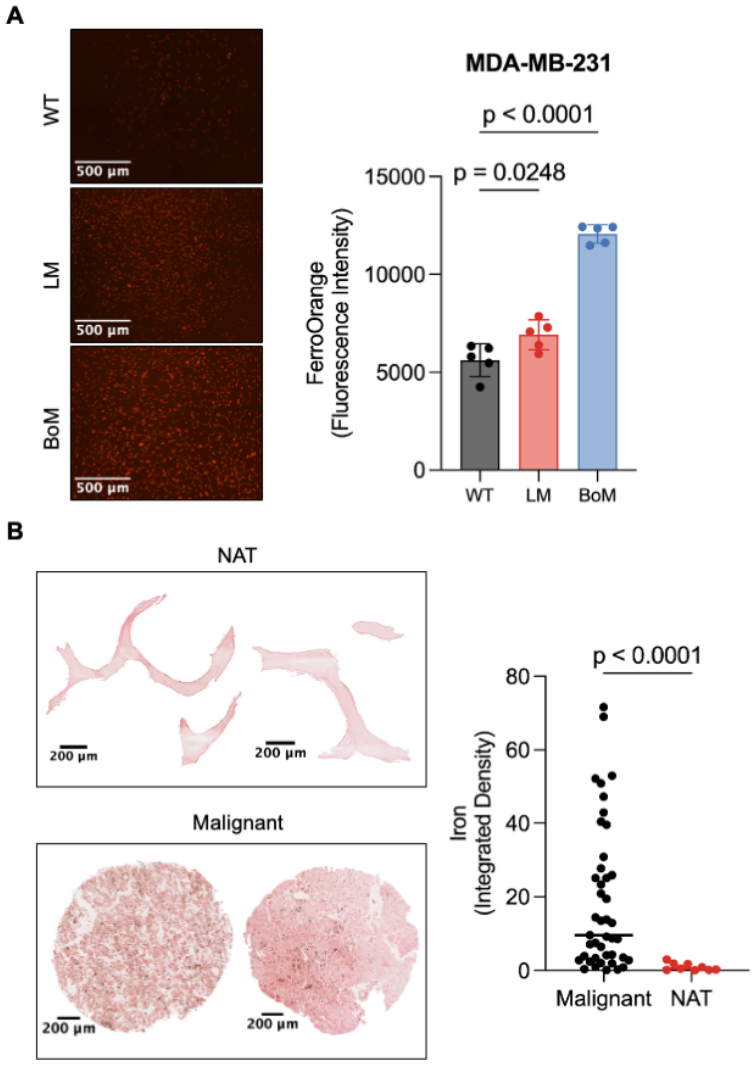


Figure 6: Intracellular iron levels in metastatic breast cancer cells and patient bone tumours.

A: *Intracellular iron levels were quantified by FerroOrange fluorescence in MDA-MB-231 WT, LM,*

and BoM cells, showing significantly elevated iron in LM and BoM cells compared to WT, with BoM cells exhibiting the highest levels. Data represent the mean of 5 technical replicates per group. Representative fluorescence images are provided for each cell line. Statistical analysis by ordinary one-way ANOVA with Dunnett's multiple comparisons test revealed a significant difference between groups ($P < 0.0001$). Dunnett's test confirmed significant increases for WT vs. LM (adjusted $p = 0.0248$) and WT vs. BoM (adjusted $p < 0.0001$). Scale bars represent 500 µm. ***B:*** *Histological iron staining of a patient bone tumour tissue microarray including various bone and cartilage malignancies and adjacent normal tissue (NAT). Malignant bone tissue ($n = 43$) exhibited significantly higher iron accumulation than NAT ($n = 9$). Statistical analysis by Mann-Whitney test confirmed this difference ($p < 0.0001$). Representative images are provided for each group. Scale bars represent 200 µm.*

Ferroptosis induction increases MHC-I expression in metastatic cells

Building on the observed suppression of MHC-I expression and antigen presentation pathways in metastatic breast cancer sublines, we next investigated whether ferroptosis induction modulates MHC-I levels in these cells. Given the increased ferroptosis sensitivity observed in metastatic cells (**Figures 4–6**), we hypothesised that pharmacological induction of ferroptosis may modulate the antigen presentation machinery.

To test this, we treated MDA-MB-231 WT, LM, and BoM cells with 2.5 µM erastin, to induce ferroptosis, or vehicle control. Western blot analysis of total MHC-I protein, using a pan-HLA-ABC antibody, confirmed that while WT cells exhibited robust MHC-I expression under basal conditions, both LM and BoM metastatic sublines showed markedly reduced baseline MHC-I protein levels, consistent with previous findings (**Figure 7A**). Interestingly, erastin treatment significantly increased MHC-I protein expression in LM and BoM cells (**Figure 7A**).

To specifically assess cell surface MHC-I expression, we performed FACS with an HLA-ABC antibody. Consistent with total protein analysis, surface MHC-I was significantly decreased in LM and BoM cells compared to WT under basal conditions (**Figure 7B**). Upon erastin treatment, surface MHC-I expression was significantly upregulated in LM and BoM cells, confirming that ferroptosis induction may upregulate MHC-I surface expression, which could enhance antigen presentation (**Figure 7B**). These data suggest that ferroptosis induction may partially restore MHC-I surface expression in metastatic breast cancer cells, with possible implications for immune recognition.

However, analysis of HLA-A2, a specific MHC-I allele recognised by Jurkat 1G4 T cells, showed an unexpected and significant decrease in cell surface expression following erastin treatment across WT, LM, and BoM cells, with LM and BoM sublines experiencing the greatest reductions (**Figure 7C**). This suggests that individual HLA alleles may be differentially regulated during ferroptosis, and that while overall MHC-I is increased, certain alleles critical for T cell recognition may not be restored. Consequently, interpretation of immune recognition after ferroptosis induction should consider these allele-specific effects.

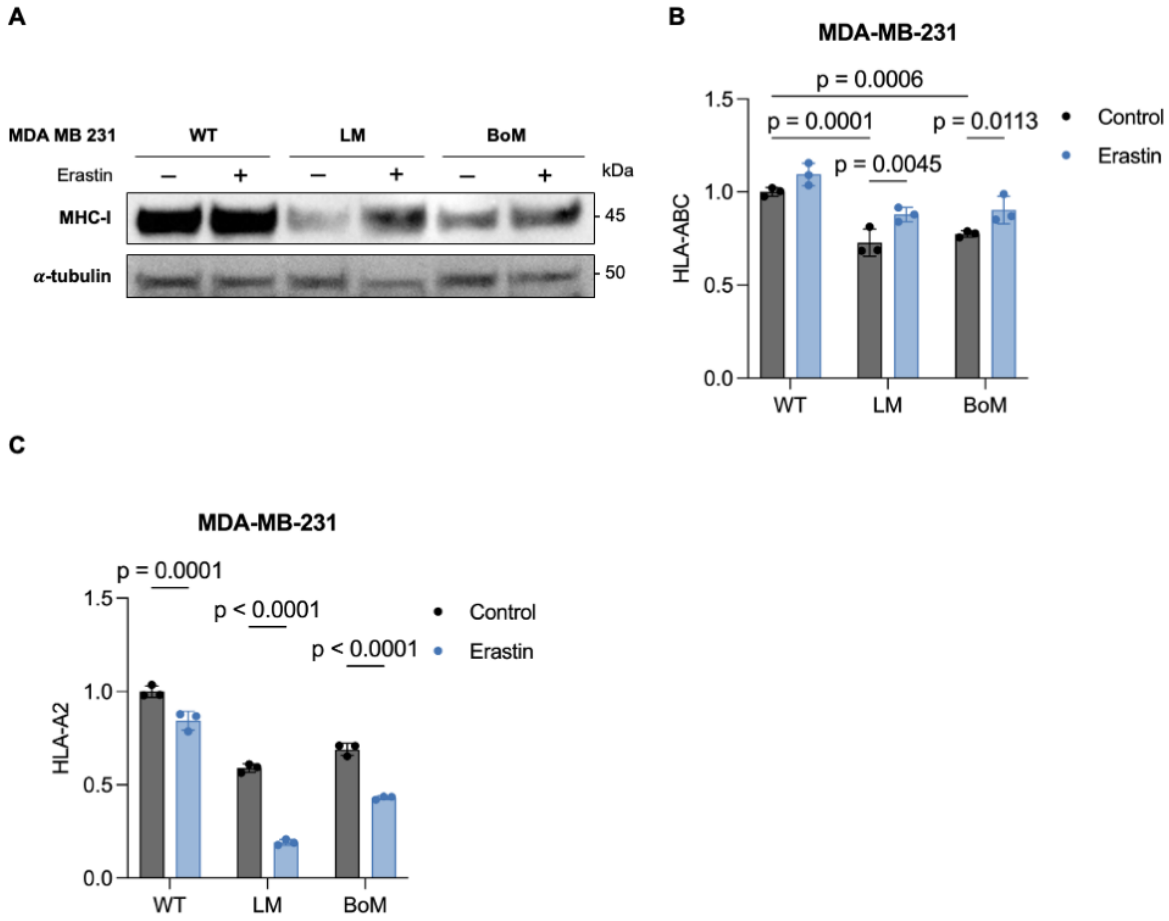


Figure 7: Ferroptosis induction increases MHC-I surface expression and differentially modulates HLA-A2 levels in metastatic breast cancer cells. A: *Western blot of total MHC-I protein (HLA-ABC antibody) in MDA-MB-231 WT, LM and BoM cells treated with vehicle or erastin (2.5 μM, 24 h). Metastatic sublines show reduced basal MHC-I levels compared to WT, which increase following erastin treatment, especially in LM cells. α-tubulin was used as loading control.* ***B-D:*** *Flow cytometry quantification of surface expression of (**B**) HLA-ABC and (**C**) HLA-A2 in WT, LM, and BoM cells treated with vehicle or erastin (2.5 μM, 24 h). Erastin treatment significantly increases HLA-ABC surface expression in LM ($p = 0.0045$) and BoM ($p = 0.0113$). Surface HLA-A2 expression significantly decreases in all sublines with erastin treatment (WT $p = 0.0001$, LM and BoM $p < 0.0001$). Statistical analysis was performed using two-way ANOVA with Šídák's multiple comparisons test. Data are shown as mean ± SD from three technical replicates.*

Ferroptosis modulates lipid peroxidation and antigen presentation in metastatic tumours

Following these *in vitro* analyses, we extended our investigation to an *in vivo* xenograft model to evaluate the effect of pharmacological induction of ferroptosis using the bioavailable SLC7A11 inhibitor imidazole ketone erastin (IKE). Mice bearing MDA-MB-231 WT, LM, or BoM xenograft tumours were randomised to receive either vehicle control or IKE administered intraperitoneally three times per week once tumours reached an average of 50 mm^3 (**Figure 8A**). LM and BoM tumours exhibited accelerated growth compared to WT, with treatment starting earlier for LM and BoM (day 18) relative to WT (day 25), as indicated by dashed lines in the tumour growth curves (**Figure 8B**). Their enhanced metastatic capacity was also supported by higher incidence of lung metastasis (**Appendix B**). However, unlike our in vitro data IKE treatment had no significant effect on tumour growth compared to vehicle control across all sublines, contrary to our hypothesis that metastatic tumours are more sensitive to ferroptosis induction (**Figure 8B**).

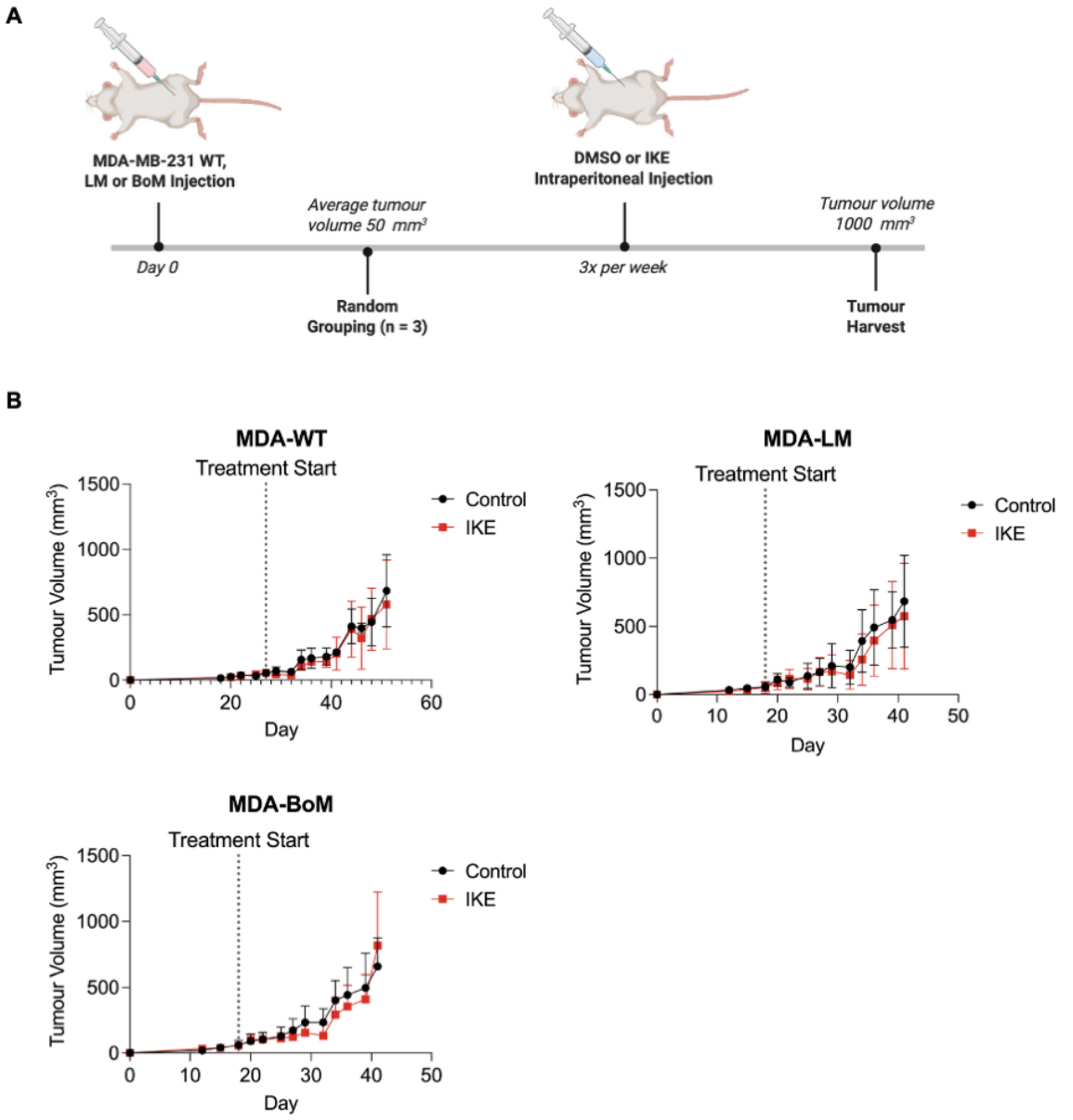


Figure 8: No effect of IKE treatment on tumour growth in MDA-MB-231 xenograft tumours. ***A:*** *MDA-MB-231 WT, LM, or BoM cells were injected into the mammary fat pad of mice, and upon reaching an average tumour volume of approximately 50 mm³, mice were randomized (n = 3 per treatment group) to receive intraperitoneal injections of vehicle control or 50 mg/kg IKE three times weekly. Tumours were harvested around 1000 mm³ for analysis.* ***B:*** *Tumour growth curves for each MDA-MB-231 subline (WT, LM, BoM) showing mean tumour volume (mm³) ± SD over time for mice treated with DMSO control or IKE. LM and BoM tumours exhibited more rapid growth, so treatment was initiated at day 18 for these groups, while treatment for WT was started at day 25 (dashed lines indicate treatment start). Tumour volumes were measured with callipers three times weekly until*

endpoint. No significant tumour regression or marked growth inhibition was observed with IKE treatment compared to control.

IHC analysis of 4HNE, revealed a significant increase in lipid peroxidation following IKE treatment in WT tumours and a non-significant trend towards increased 4HNE in BoM tumours, although the small sample size per treatment group limits definitive conclusions (**Figure 9**). At baseline, although LM tumours exhibited higher 4HNE staining compared to WT, no further induction was observed by IKE (**Figure 9**). The lack of a significantly increased 4HNE response in LM and BoM tumours following IKE treatment may reflect the inability of IKE to slow the faster-growing LM and BoM tumours, in contrast to the slower-growing WT tumours where the treatment effect on lipid peroxidation is more detectable (**Figure 9**).

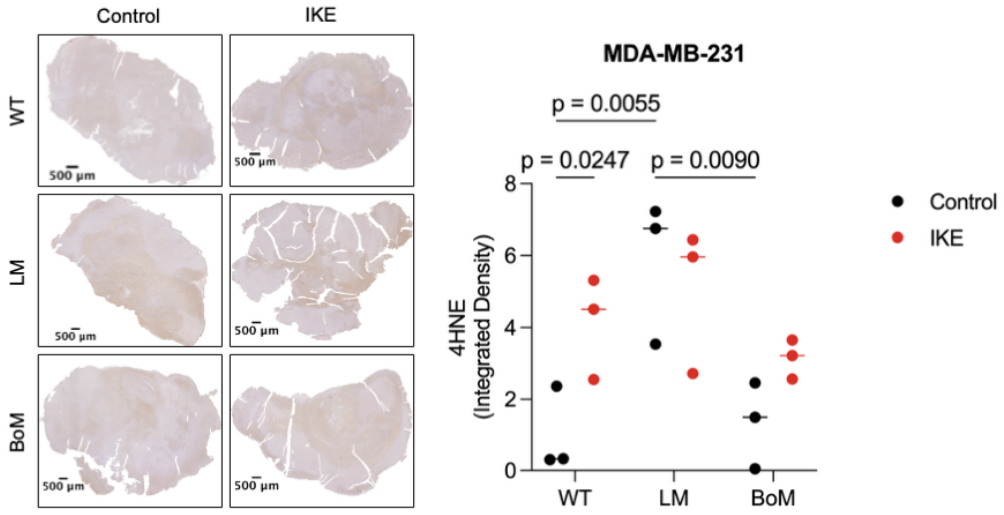


Figure 9: Lipid peroxidation changes in MDA-MB-231 WT and metastatic xenograft tumours following IKE treatment in a pilot study*. Representative 4-hydroxynonenal (4HNE) immunohistochemical staining of WT, LM, and BoM tumour sections from control and IKE-treated mice are shown. Scale bars represent 500 µm. Quantification of 4HNE integrated density demonstrated a significant increase in lipid peroxidation following IKE treatment in WT tumours, with a non-significant trend towards increased 4HNE in BoM tumours. At baseline, control LM tumours had significantly higher 4HNE levels than WT and BoM tumours, while BoM tumours showed a non-*

significant trend towards higher 4HNE compared to WT. Each data point represents an individual tumour (n = 3 per treatment group). Statistical analysis was performed using two-way ANOVA with Šídák's multiple comparisons test; with significant comparisons indicated on the graph. Bars represent median intensity.

Following the *in vitro* findings of ferroptosis-induced modulation of MHC-I expression, we next assessed whether pharmacological induction of ferroptosis with IKE similarly alters MHC-I levels *in vivo*. Using the same MDA-MB-231 WT, LM, and BoM xenograft mouse model outlined in **Figure 8A**, tumour sections were examined for MHC-I (HLA-ABC) expression by IHC. It is important to note that this xenograft model is immunocompromised, and while it allows assessment of tumour-intrinsic effects, the absence of an intact immune system limits the ability to fully recapitulate the tumour–immune interactions that may influence MHC-I regulation.

In contrast to *in vitro* results, baseline MHC-I staining intensity was uniformly low across WT, LM, and BoM tumours in DMSO-treated mice (**Figure 10**). *In vitro* we observe high MHC-I expression in WT cells (**Figure 2B**), but it may be possible that this expression changes with tumour progression *in vivo*. Interestingly, IKE treatment significantly increased MHC-I expression in WT and BoM tumours, aligning with our *in vitro* observation that ferroptosis induction enhances MHC-I levels (**Figure 10**). However, LM tumours did not exhibit this increase and remained low despite treatment (**Figure 10**). Due to the pilot nature and limited sample size (n = 3), these findings require cautious interpretation and further detailed investigation. Future studies in immunocompetent models would help clarify how ferroptosis induction affects antigen presentation within an intact immune system and better reflect the physiological tumour microenvironment.

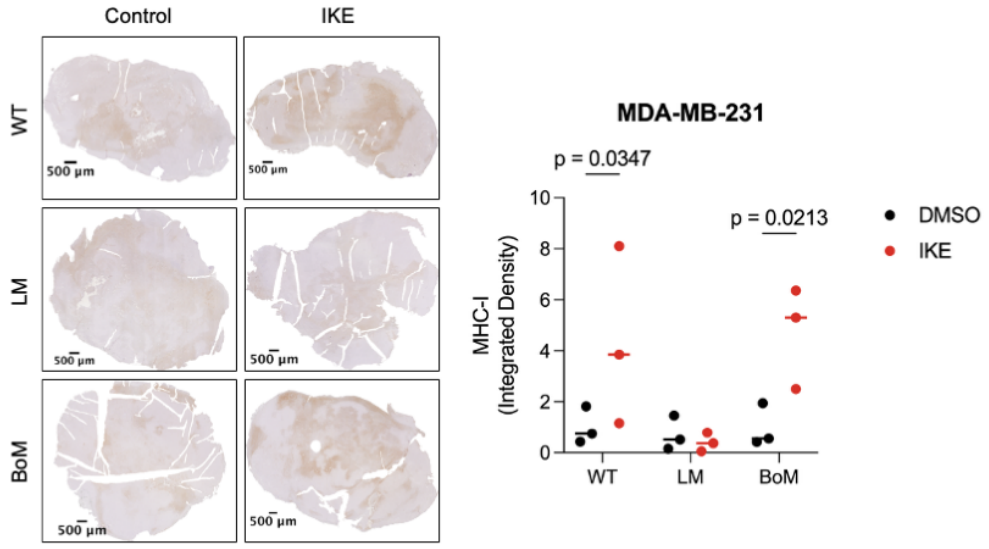


Figure 10: IKE treatment increases MHC-I expression in primary and bone metastatic tumours in vivo. *Representative IHC staining of MHC-I (HLA-ABC) in whole tumour sections from MDA-MB-231 WT, LM, and BoM xenografts treated with vehicle or IKE. Scale bars represent 500 µm. Quantification of MHC-I staining intensity (integrated density) shows significant increases following IKE treatment in WT (p = 0.0347) and BoM (p = 0.0213) tumours, with no significant change observed in LM tumours. Each data point represents an individual tumour (n = 3 per treatment group). Statistical analysis was performed using two-way ANOVA with Šídák's multiple comparisons test; with significant comparisons indicated on the graph. Bars represent median intensity.*

Discussion

This study provides new insights into the role of ferroptosis in metastatic breast cancer, particularly to the lung and bone, by addressing key molecular and functional differences between metastatic and primary tumour cells. Our results demonstrate that lung- and bone-metastatic sublines of MDA-MB-231 breast cancer cells exhibit suppressed ferroptosis defence and antigen presentation pathways, resulting in enhanced sensitivity to ferroptotic stress while suppressing T cell-mediated cell death through changes in MHC-I expression. Interestingly, induction of ferroptosis partially restores MHC-I expression in metastatic cells, suggesting a novel link between cell death pathways and

immune surveillance. Collectively, these findings are the first to characterise ferroptosis vulnerabilities and their immune consequences in preclinical models of breast cancer metastasis to both lung and bone. Importantly, these discoveries align with our study's aims to identify molecular characteristics, examine ferroptosis sensitivity, and explore antigen presentation dynamics in metastatic breast cancer. Together, they provide insight into the cellular and molecular features that characterise metastatic behaviour and highlight new directions for future research in this challenging setting.

Molecular characteristics of metastatic breast cancer cells

Understanding the molecular characteristics of metastatic breast cancer cells is crucial for elucidating how these cells adapt to distant organs such as bone and lung, ultimately shaping disease progression. By analysing a previously generated RNA sequencing dataset from our group, comparing wild-type (WT) MDA-MB-231 cells with their lung (LM) and bone (BoM) metastatic sublines, we found that metastatic cell lines exhibit consistently downregulated antigen presentation and ferroptosis defence pathways (**Figure 2**). Protein and immunofluorescence analyses confirmed reduced MHC-I expression in metastatic cells, and functional T cell activation assays indicated a trend toward impaired immune recognition (**Figure 2, Figure 3**). Collectively, these results suggest that metastatic breast cancer cells possess intrinsic molecular characteristics that may facilitate immune evasion and altered ferroptosis sensitivity.

Downregulation of MHC-I is a well-established mechanism by which tumours evade cytotoxic T cell-mediated immunity, facilitating immune escape and metastatic progression (Cornel et al., 2020, Taylor and Balko, 2022). Tumour-specific MHC-I loss correlates with poorer prognosis and resistance to immunotherapies across multiple cancer types, including breast cancer (Taylor and Balko, 2022). Reduced antigen presentation can arise from diverse mechanisms, such as genetic alterations, transcriptional repression, or epigenetic modifications, collectively resulting in defective tumour antigen display (Cornel

et al., 2020, Kong et al., 2025). This loss allows metastatic cancer cells to escape immune surveillance by evading $CD8^+$ T cell recognition, a known adaptive feature of advanced breast cancer (Dhatchinamoorthy et al., 2021). Our experimental data provide functional evidence linking decreased MHC-I expression to reduced T cell activation, supporting the biological significance of MHC-I downregulation in metastatic immune evasion.

In parallel, analysis of consistently downregulated genes in lung and bone metastatic cells revealed suppression of ferroptosis defence pathways compared to parental cells (**Figure 2**). Protein validation confirmed notably decreased SLC7A11 expression, which maintains cellular redox balance by importing cystine for glutathione synthesis and lipid peroxide detoxification (**Figure 2**) (Dixon et al., 2012). GPX4, another key ferroptosis suppressor that directly detoxifies lipid peroxides, was also reduced (Yang et al., 2014). Interestingly, GPX4 reduction was less pronounced in BoM cells compared to LM. Transferrin, an iron transporter that can influence ferroptosis sensitivity through cellular iron availability, remained unchanged, suggesting that the observed alterations in ferroptosis defence are primarily driven by reduced antioxidant capacity rather than altered iron uptake (Dixon et al., 2012). Previous studies have shown that while many tumours upregulate SLC7A11 and GPX4 to evade ferroptosis, disruption of this antioxidant defence can render cells highly vulnerable to oxidative stress, particularly within metabolically challenging microenvironments (Lei et al., 2022a). These findings suggest that reduced ferroptosis defence in the LM and BoM sublines may represent a therapeutic vulnerability.

Enhanced ferroptosis sensitivity in metastatic sublines

Following the observed downregulation of ferroptosis defence pathways and decreased SLC7A11 expression in lung and bone metastatic sublines, we found that these cells exhibited increased sensitivity to ferroptosis compared with WT cells (**Figure 4**). This heightened vulnerability suggests that metastatic breast cancer cells may possess intrinsic

molecular adaptations that render them more susceptible to ferroptotic stress, highlighting potential therapeutic opportunities.

This enhanced ferroptosis sensitivity aligns with current literature which has established that aggressive, therapy-resistant and metastatic cancer cells, often displaying mesenchymal plasticity, are broadly vulnerable to ferroptosis due to specific metabolic rewiring. For example, Viswanathan et al. (2017) discovered that therapy-resistant, high-mesenchymal state cancer cells become dependent on GPX4 to neutralise the lipid peroxides that accumulate due to increased PUFA content, resulting in a strict reliance on lipid peroxidase defence and heightened ferroptosis vulnerability. This dependency is driven by EMT-linked transcriptional reprogramming, particularly by ZEB1 (Zinc finger E-box-binding homeobox 1) (Viswanathan et al., 2017). Building on these findings, Schwab et al. (2024) demonstrated that ZEB1 directly orchestrates ferroptosis sensitivity by promoting PUFA synthesis and suppressing MUFA production, thus predisposing metastatic and plastic tumour cells to lethal lipid peroxidation. These studies highlight how metastatic progression and cell state plasticity can create specific ferroptosis vulnerabilities (Viswanathan et al., 2017, Schwab et al., 2024).

Adding to this, recent investigations have identified a particular susceptibility of TNBC to ferroptosis, linked to its distinct metabolic profile and molecular characteristics. Verma et al. (2020) revealed that pharmacological induction of ferroptosis in TNBC cells is associated with increased cellular iron and decreased glutathione levels, particularly through reduced expression of GPX4 and key glutathione biosynthesis genes, highlighting a natural vulnerability via disruption of antioxidant defences. Furthermore, Doll et al. (2017) identified acyl-CoA synthetase long-chain family member 4 (ACSL4) as an essential enzyme for ferroptosis execution, preferentially expressed in basal-like breast cancer subtypes of TNBC, enabling enrichment of long-chain PUFAs in cellular membranes that fuel ferroptotic lipid peroxidation. These insights suggest that the unique metabolic adaptations of TNBC

render it particularly sensitive to ferroptosis induction, marking it as a particularly promising target for therapeutic intervention.

Having established increased ferroptosis sensitivity in metastatic cells, this vulnerability was further supported by their increased accumulation of lipid peroxides following erastin treatment, a defining feature of ferroptotic stress (**Figure 5**) (Dixon et al., 2012). The fold change in lipid peroxidation was particularly pronounced in LM and BoM cells compared to WT cells, suggesting heightened susceptibility to oxidative lipid damage in metastatic sublines. (**Figure 5**). The increased erastin-induced lipid peroxidation observed in metastatic sublines may partly reflect reduced SLC7A11 expression, which limits cystine uptake and glutathione synthesis capacity (Dixon et al., 2012). However, considering that tumour cells in circulation and metastatic sites often face elevated oxidative stress, they likely employ compensatory mechanisms to maintain redox balance, which could include upregulating other antioxidant defences such as GPX4 (Yang et al., 2014, Hua et al., 2024). Interestingly, we observe that GPX4 reduction is less pronounced in BoM cells compared to LM (**Figure 2**), which may reflect a compensatory mechanism in BoM to counteract the higher lipid peroxidation observed following erastin treatment (**Figure 5**). Besides these well-characterised defences, emerging evidence also suggests that cancer cells can acquire cysteine through alternative pathways such as de novo synthesis via the transsulfuration pathway, uptake by non-specific amino acid transporters, or protein scavenging through micropinocytosis (Bonifácio et al., 2021, Byun et al., 2022, Zhang et al., 2022). These metabolic adaptations provide potential routes for cysteine supply independent of SLC7A11 and GPX4 activity and warrant further investigation to clarify their roles in metastatic cell survival under ferroptotic stress (Bonifácio et al., 2021).

The elevated erastin-induced lipid peroxidation we observed in metastatic cells aligns with recent work demonstrating the centrality of tumour lipid metabolism in ferroptosis sensitivity. Studies reveal that high activity of fatty acid desaturases (FADS1/2) promote PUFA

biosynthesis and ferroptosis susceptibility in triple-negative breast cancer and other aggressive subtypes (Lorito et al., 2024). Moreover, tumour microenvironmental acidosis, common in rapidly growing and metastatic tumours, potentiates PUFA peroxidation and the cytotoxic effects of ferroptosis (Dierge et al., 2021). This microenvironmental driver may act in concert with intrinsic metabolic rewiring to further increase metastatic cell sensitivity (Dierge et al., 2021, Riemann et al., 2016).

Since iron catalyses the formation of ROS through Fenton chemistry, it plays a key role in promoting the lipid peroxidation that drives ferroptosis (Dixon et al., 2012). To assess whether altered iron homeostasis contributes to the heightened ferroptotic vulnerability of metastatic cells, we measured intracellular iron and found that both LM and BoM cells exhibited increased iron levels, with BoM cells showing the highest levels (**Figure 6**). This is consistent with evidence that cancer cells, including those in metastatic or therapy-resistant states, often subvert iron metabolism to meet proliferative and metabolic demands (Torti et al., 2018). Increased iron not only fosters tumour growth but can also enhance metastatic potential by promoting oxidative stress and susceptibility to ferroptosis (Torti et al., 2018, Hann et al., 1991). Notably, metastatic breast cancer has been specifically associated with elevated serum ferritin and iron, supporting a systemic iron dysregulation in advanced disease (Marcus and Zinberg, 1975). Elevated iron increases the rate of lipid peroxidation, further predisposing metastatic cells to ferroptotic death.

We further investigated whether this elevation is reflected in patient samples by analysing iron staining in a bone tissue microarray, comparing malignant bone tumours (such as osteosarcoma and multiple myeloma) with normal adjacent tissue (NAT) controls. Malignant bone tumours displayed significantly higher iron, consistent with the *in vitro* findings (**Figure 6**). These observations suggest that malignant bone tumours may alter iron metabolism to increase intracellular iron. This aligns with the observation that high expression of transferrin receptor-1 (TfR1), a principal iron uptake protein, has been reported in

aggressive bone tumours, where it correlates with histologic grade, metastasis, and poorer overall survival (Wu et al., 2019). TfR1 is critical in ferroptosis because it facilitates cellular iron uptake, increasing the labile iron pool that catalyses lipid peroxidation and promotes ferroptotic cell death (Feng et al., 2020). Although further studies are required using clinically relevant breast cancer samples, these findings support the idea that iron accumulation in bone residing tumours may act as a key driver of ferroptosis sensitivity.

Collectively, these results highlight that metastatic sublines display increased ferroptosis sensitivity, which may be influenced by intrinsic metabolic rewiring, iron accumulation, and altered lipid metabolism. While these findings reveal a potential vulnerability in metastatic cells, further research is required to determine whether this ferroptosis sensitivity can be effectively exploited *in vivo* and whether it might inform novel therapeutic strategies for aggressive metastatic breast cancer.

Ferroptosis induction and modulation of antigen presentation

The observation that metastatic breast cancer sublines downregulate MHC-I while also displaying heightened sensitivity to ferroptosis raises the possibility of an intersection between these processes. In this study, ferroptosis induction with erastin was associated with an increase in both total and surface MHC-I in lung and bone metastatic cells, which otherwise exhibited very low basal expression (**Figure 7)**. These findings suggest that ferroptotic stress may counteract, at least in part, the loss of antigen presentation that characterises metastatic progression.

Previous reports show that ferroptosis can have divergent immunological consequences depending on its stage. It has been demonstrated that late stage ferroptotic cells, despite releasing classical DAMPs such as High Mobility Group Box 1 protein (HMGB1) and calreticulin, can suppress rather than stimulate immune responses (Wiernicki et al., 2022).

This immunosuppression is thought to arise from the accumulation of lipid peroxidation products, which interfere with dendritic cell function (Wiernicki et al., 2022). Oxidised lipids impair peptide loading onto MHC-I complexes, thereby disrupting cross-presentation and reducing $CD8^+$ T-cell activation (Ramakrishnan et al., 2014). In HPV-driven cervical cancer models, where redox stress is already a defining feature, the induction of ferroptosis has been shown to exacerbate defects in the MHC-I antigen presentation pathway (Li et al., 2025). Rather than enhancing immune visibility, it has been shown that lipid peroxidation and oxidative imbalance disrupt the processing and trafficking of MHC-I, thereby facilitating tumour immune evasion (Li et al., 2025). Moreover, mitochondrial dynamics and endoplasmic reticulum (ER) stress have been implicated in MHC-I regulation, where mitochondrial fission and prolonged ER stress reduce MHC-I surface expression (Lei et al., 2022b).

Importantly, lipid peroxidation is not universally detrimental for antigen presentation. A recent study demonstrated that during immune synapse formation, licensed dendritic cells undergo controlled lipid peroxidation alongside upregulation of MHC-I, enabling efficient priming of $CD8^+$ T-cell responses (Calzada-Fraile et al., 2023). In line with this, ferroptosis has been highlighted as a potential means of boosting antitumour immunity, particularly when combined with immune checkpoint blockade, where it may help to overcome resistance and broaden patient responses (Dang et al., 2022).

Overall, these results provide preliminary evidence that ferroptosis induction may enhance MHC-I-mediated antigen presentation in metastatic breast cancer cells with suppressed basal MHC-I expression, but this effect may be context-dependent. This raises the intriguing possibility that ferroptosis-inducing therapies could not only exploit metabolic vulnerabilities of metastatic cells but also modulate anti-tumour immune responses.

Building on our observations that total MHC-I levels can increase following ferroptosis induction, we next examined the regulation of a specific MHC-I allele to better understand how ferroptotic stress influences antigen presentation. We focused on HLA-A2, as this allele is recognised by Jurkat 1G4 T cells (**Figure 3**). Interestingly, although HLA-A2 levels were lower in control-treated metastatic cells compared to WT, ferroptosis induction with erastin resulted in a further significant decrease in surface HLA-A2 expression across WT, LM, and BoM cells (**Figure 7**). Our finding that basal HLA-A2 levels were lower in metastatic cells compared with parental WT cells, is consistent with previous observations of allele-specific HLA-A2 loss in melanoma as a mechanism of immune evasion (Maeurer et al., 1996). Previous studies have investigated ferroptosis in the context of total MHC-I but did not report allele-specific effects (Calzada-Fraile et al., 2023, Lei et al., 2022b, Li et al., 2025, Ramakrishnan et al., 2014, Wiernicki et al., 2022). To our knowledge, this is the first report demonstrating allele-specific modulation of MHC-I by ferroptosis.

These findings collectively highlight that ferroptotic stress exerts allele-specific effects on MHC-I expression. While total MHC-I can be partially restored in metastatic cells, HLA-A2 may be selectively downregulated. This differential regulation could have functional consequences for T cell recognition and immune evasion in metastatic breast cancer and suggests that future studies should consider the allele-specific context when evaluating immune responses under ferroptotic conditions.

Ferroptosis induction alters lipid peroxidation and antigen presentation *in vivo*

To further investigate whether the ferroptosis-related vulnerabilities identified *in vitro* are recapitulated *in vivo*, we performed a pilot study using NSG mice injected orthotopically with parental, LM, and BoM cells into the mammary fat pad.

We assessed the effect of pharmacological induction of ferroptosis using imidazole ketone erastin (IKE), a well-characterised bioavailable SLC7A11 inhibitor widely used *in vivo* to induce ferroptosis (Larraufie et al., 2015, Zhang et al., 2019b). Recent studies have demonstrated that RSL3, a potent inhibitor of GPX4, effectively induces ferroptosis *in vivo* in metastatic breast cancer models (Lorito et al., 2024, Yuan et al., 2025, Yang et al., 2014). Despite this, our preference for IKE in our *in vivo* pilot study was guided by concerns about the potential toxicities of RSL3. IKE offers improved metabolic stability and solubility, representing a promising ferroptosis inducer for therapeutic development (Larraufie et al., 2015, Zhang et al., 2019b). Comparative studies are needed to better understand the relative safety and efficacy of these compounds as ferroptosis inducers in breast cancer models.

Despite our in vitro findings that metastatic cells exhibit heightened sensitivity to ferroptosis, IKE treatment did not reduce tumour growth in any group (**Figure 8**). Several factors may account for the lack of detectable tumour growth inhibition. First, only a single IKE concentration and a three-times-per-week dosing schedule were used; more frequent administration or alternative dosing may be necessary to achieve sufficient intratumoural exposure. Second, IKE pharmacokinetics and bioavailability in metastatic breast cancer xenografts remain incompletely characterised, which may limit its efficacy *in vivo* (Zhang et al., 2019b). Third, the faster growth of LM and BoM tumours may have shortened the time window in which ferroptosis induction could effectively occur. Importantly, previous studies have highlighted the challenges of inducing ferroptosis effectively *in vivo*, due to pharmacological limitations of current compounds and the complex tumour microenvironment, underscoring the need for improved ferroptosis inducers with better bioavailability and potency (Zhang et al., 2019b, Zou and Schreiber, 2020).

IHC analysis of tumours sections stained for 4HNE indeed revealed that WT tumours, which grew more slowly, displayed a significant increase in 4HNE following IKE treatment,

whereas LM and BoM tumours exhibited only a non-significant trend, suggesting that tumour growth dynamics and metabolic state influence the *in vivo* ferroptotic response (**Figure 9**). Importantly, tumour microenvironmental factors, including stromal interactions, oxidative stress, and nutrient availability, may modulate ferroptosis sensitivity *in vivo* and are not fully recapitulated *in vitro* (Hua et al., 2024). Furthermore, the small sample size in this pilot study (n = 3 per treatment group) warrants cautious interpretation and underscores the need for further experiments with increased cohort sizes to validate these findings. Taken together, these observations indicate that while IKE is capable of inducing lipid peroxidation, achieving a robust therapeutic effect may require optimisation of dosing, alternative ferroptosis inducers, or combination approaches to overcome protective microenvironmental influences. Future studies should explore these strategies and evaluate whether ferroptosis induction can be effectively harnessed to target metastatic breast cancer *in vivo*.

Following the in vitro evidence that ferroptosis induction can influence MHC-I expression, the *in vivo* xenograft experiments offer insights into how these processes might operate within a tumour environment. In vehicle-treated tumours, MHC-I staining was low across all three sublines, in contrast to the higher expression observed in parental WT cells *in vitro* (**Figure 10**). This difference between culture and xenograft conditions may reflect tumour adaptation *in vivo*, as microenvironmental cues and immune pressures are known to drive downregulation of antigen presentation (Dhatchinamoorthy et al., 2021, Yang et al., 2023). The use of immunocompromised mice in these studies may also have contributed to the low baseline MHC-I expression observed, since the absence of functional immune surveillance reduces selective pressure to maintain antigen presentation (Koyama and Hill, 2021).

IKE treatment was associated with increased MHC-I expression in WT and BoM tumours, consistent with the idea that ferroptotic stress can enhance antigen presentation under

certain conditions (**Figure 10**). In contrast, LM tumours did not show an increase and remained low after treatment (**Figure 10**). Importantly, *in vitro* experiments established that ferroptosis induction significantly increased MHC-I expression in both LM and BoM cell lines, which displayed low baseline levels. However, this upregulation was not recapitulated *in vivo* in LM tumours, illustrating how the tumour microenvironment and additional context-dependent factors may constrain the immunogenic effects of ferroptosis observed in cell culture (Catanzaro et al., 2024).

Together, these findings suggest that the impact of ferroptosis on MHC-I expression may depend on tumour context and metastatic state, raising the possibility that ferroptosis inducers could modulate not only tumour survival but also tumour–immune interactions. However, interpretation is constrained by the use of immunocompromised mice and the small sample size (n = 3 per group). Future studies in immunocompetent models, with larger cohorts and analysis of both primary and metastatic lesions, will be essential to determine whether increased MHC-I expression after ferroptosis induction translates into enhanced recognition by cytotoxic T cells. Such studies could help establish whether ferroptosis inducers might be useful in combination with immunotherapies, particularly in metastatic cancers where immune evasion is a dominant feature.

Therapeutic implications

The demonstrated ferroptosis vulnerability of lung and bone metastatic breast cancer sublines highlights ferroptosis induction as a promising therapeutic strategy specifically targeting metastatic disease. The observation of reduced ferroptosis defence, increased intracellular iron, and heightened lipid peroxidation in metastatic cells create a metabolic liability that could be exploited pharmacologically (Dixon et al., 2012, Lei et al., 2022a). While erastin effectively induces ferroptosis *in vitro*, translation of ferroptosis induction into *in vivo* contexts using IKE has faced challenges. Our findings that IKE treatment failed to

significantly inhibit tumour growth *in vivo* despite its known pharmacological stability and potency highlight the need for optimisation of dosing, delivery, and compound properties to overcome tumour microenvironmental barriers and heterogeneity (Larraufie et al., 2015, Zhang et al., 2019b).

Moreover, the observed modulation of antigen presentation by ferroptosis induction suggests a potential synergy between ferroptosis inducers and immunotherapies. Restoration of MHC-I surface expression in metastatic cells following ferroptotic stress could enhance tumour immunogenicity and promote cytotoxic T cell recognition, thereby overcoming immune evasion (Dhatchinamoorthy et al., 2021). However, differential regulation of MHC-I alleles such as the decrease in HLA-A2 indicates complexity that may impact T cell responses and necessitates allele-specific considerations in therapeutic design. The integration of ferroptosis induction with immunotherapies, such as immune checkpoint inhibitors, holds promise as a complementary approach that may enhance elimination of metastatic cells by combining metabolic disruption with increased immune surveillance. Emerging evidence indicates potential synergy between these modalities, although further research is required to clarify the underlying mechanisms and therapeutic applicability (Dang et al., 2022).

Limitations and future directions

This study has several limitations that should be acknowledged. Firstly, the *in vivo* experiments were conducted with a small number of animals (n = 3 per treatment group), which limits the statistical power and may have reduced the ability to detect subtle but biologically relevant effects of ferroptosis induction on tumour growth. To address this, future studies should incorporate larger cohorts to confirm and expand on these findings.

Secondly, the use of immune-deficient NSG mouse models restricts the investigation of ferroptosis within the context of a fully functional immune system. This limits the ability to assess complex tumour-immune interactions, including how ferroptotic stress influences antigen presentation, immune cell activation, and cytotoxic responses in metastatic niches. Therefore, incorporating immune-competent *in vivo* models in future research will be essential to more fully understand these mechanisms and their therapeutic implications.

Thirdly, the *in vitro* assays, although informative, do not fully recapitulate the complexity of the tumour microenvironment. Key components such as stromal cells, immune infiltrates, and metabolic heterogeneity are absent, which likely influence ferroptosis sensitivity and antigen presentation dynamics *in vivo* (Hua et al., 2024). Follow-up studies employing more physiologically relevant co-culture systems may provide deeper insights into these interactions.

Additionally, the allele-specific regulation of MHC-I observed following ferroptosis induction introduces further complexity to the interpretation of antigen presentation changes. Current analyses provide limited insight into the functional implications of differential MHC-I allele modulation, underscoring the need for additional research focusing on allele-specific antigen presentation and its role in immune recognition.

Finally, the pharmacokinetic properties and dosing schedule of the ferroptosis inducer, IKE, used in this study may not have achieved optimal ferroptotic effects *in vivo*. This, combined with the rapid growth of metastatic tumours, may have contributed to the lack of significant tumour growth inhibition observed. Further optimisation of dosing regimens and pharmacodynamic characterisation of ferroptosis inducers will be important in future therapeutic development.

Considering these limitations, the findings primarily reflect the behaviour of the lung and bone metastatic sublines derived from MDA-MB-231 cells and may not be fully generalisable across other breast cancer subtypes or metastatic sites. Expanding experimental models to include diverse breast cancer subtypes and metastatic niches will enhance the translational relevance and applicability of future investigations.

Taken together, these limitations highlight key areas where further research is needed to deepen understanding and improve therapeutic strategies. Addressing these challenges through expanded models, larger cohorts, and more physiologically relevant systems will be critical in advancing ferroptosis-based treatments for metastatic breast cancer. The insights gained from this study provide a valuable foundation for such continued investigations.

Conclusion

This study reveals that lung and bone metastatic breast cancer cells exhibit suppressed ferroptosis defence and antigen presentation, which results in enhanced ferroptotic sensitivity and altered immune recognition. Pharmacological induction of ferroptosis partially restores MHC-I expression, suggesting a novel vulnerability that could be therapeutically exploited. While preliminary *in vivo* data are constrained by study size, these findings illustrate the complex relationship between metabolic stress and immune modulation in metastasis. Future research employing immune-competent models and focusing on antigen presentation regulation will be critical to harness ferroptosis as a strategy to improve outcomes in metastatic breast cancer.

Appendix A: Individual enrichment plots for LM and BoM sublines

Individual pathway enrichment analyses were performed for LM versus WT and BoM versus WT sublines to illustrate the contribution of each metastatic cell line to the consistently downregulated pathways identified in **Figure 2A**. Genes exhibiting reduced expression in each subline relative to WT were used for functional clustering using the DAVID tool (Huang et al., 2009), and enrichment plots display enrichment scores along with statistical significance for selected pathways. Antigen presentation and ferroptosis defence pathways were specifically examined in line with our study aims. Both LM and BoM sublines show similar patterns of downregulation in these pathways, confirming that the combined analysis in **Figure 2A** accurately reflects the contribution of each metastatic subline.

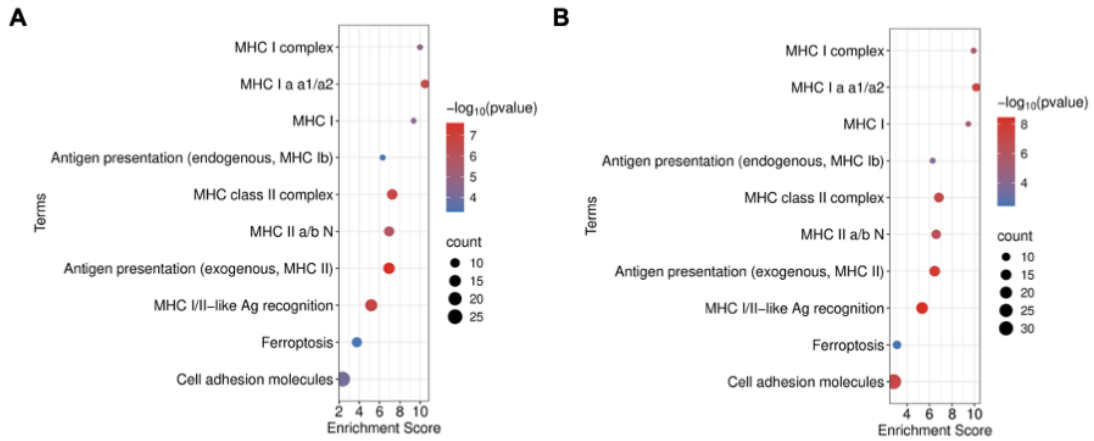


Figure A1. Individual enrichment plots for LM and BoM metastatic sublines compared with WT cells. *DAVID enrichment analysis was performed on genes downregulated in each metastatic subline relative to WT MDA-MB-231 cells. Panel (**A**) shows LM versus WT, and panel (**B**) shows BoM versus WT. Selected pathways related to antigen presentation and ferroptosis defence were highlighted in line with the study aims. Enrichment scores and statistical significance for each pathway are shown, illustrating the contribution of each subline to the combined analysis presented in **Figure 2A**.*

Appendix B: H&E staining of lungs from IKE-treated and control mice

Haematoxylin and eosin (H&E) staining was performed on lung sections from mice with WT, LM or BoM tumours in the IKE treatment study (n = 3 per treatment group) (**Figure 8A**). These images were not quantified but are shown to demonstrate the presence of metastatic lesions across the treatment groups, with LM showing the highest incidence (**Figure B1**).

H&E staining reveals lung metastases in control and IKE-treated mice

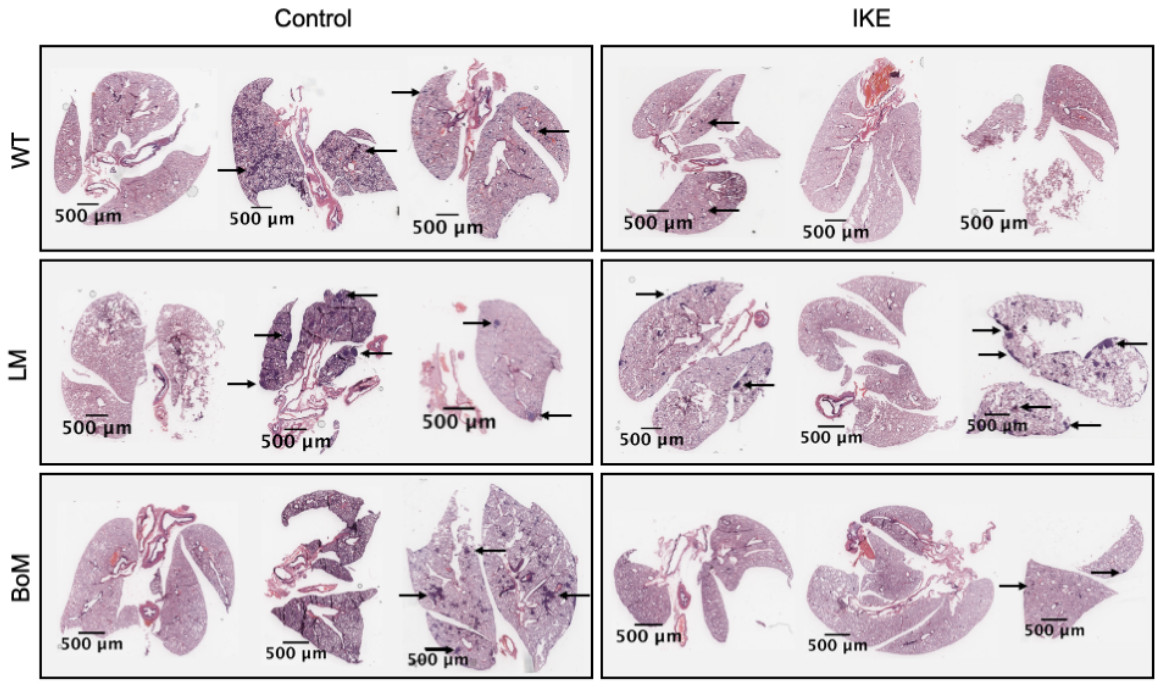


Figure B1: H&E staining reveals lung metastases in control and IKE-treated mice. *Haematoxylin and eosin (H&E) staining of WT, LM, and BoM lung sections from control and IKE-treated mice (n = 3 per treatment group). Lungs were collected at study endpoint to assess metastatic lesions. Metastases were observed in all groups, with LM showing the highest incidence. Scale bars represent 500 µm.*

Method

Paraffin-embedded lung sections were deparaffinised and rehydrated through graded alcohols. Sections were stained with 25% Harris' haematoxylin (CODE) diluted in water for

5 min and then washed under running tap water for 5 min. Slides were dipped 5 times in acid alcohol (1% hydrochloric acid in 70% ethanol), rinsed in tap water, and then dipped 10 times in Scott's tap water substitute followed by another rinse in tap water. Sections were next dipped 10 times in 0.5% lithium carbonate, rinsed in tap water, and then dipped 10 times in 50%, 70%, and 90% ethanol. Slides were counterstained with alcoholic eosin for 1 s, followed by 5 dips in 90% ethanol, repeated in fresh 90% ethanol. Finally, sections were dehydrated in 100% ethanol, followed by 2 changes of xylene, and mounted with DPX.

References

Altorki, N. K., Markowitz, G. J., Gao, D., Port, J. L., Saxena, A., Stiles, B., Mcgraw, T. & Mittal, V. 2019. The lung microenvironment: an important regulator of tumour growth and metastasis. *Nature Reviews Cancer,* 19**,** 9-31.

Balkwill, F. 2004. Cancer and the chemokine network. *Nature Reviews Cancer,* 4**,** 540-550.

Bhardwaj, V. & He, J. 2020. Reactive Oxygen Species, Metabolic Plasticity, and Drug Resistance in Cancer. *Int J Mol Sci,* 21.

Bolamperti, S., Villa, I. & Rubinacci, A. 2022. Bone remodeling: an operational process ensuring survival and bone mechanical competence. *Bone Research,* 10**,** 48.

Bonifácio, V. D. B., Pereira, S. A., Serpa, J. & Vicente, J. B. 2021. Cysteine metabolic circuitries: druggable targets in cancer. *British Journal of Cancer,* 124**,** 862-879.

Buijs, J. T. & Van Der Pluijm, G. 2009. Osteotropic cancers: From primary tumor to bone. *Cancer Letters,* 273**,** 177-193.

Burstein, H. J., Curigliano, G., Thürlimann, B., Weber, W. P., Poortmans, P., Regan, M. M., Senn, H. J., Winer, E. P., Gnant, M., Aebi, S., André, F., Barrios, C., Bergh, J., Bonnefoi, H., Bretel Morales, D., Brucker, S., Burstein, H., Cameron, D., Cardoso, F., Carey, L., Chua, B., Ciruelos, E., Colleoni, M., Curigliano, G., Delaloge, S., Denkert, C., Dubsky, P., Ejlertsen, B., Fitzal, F., Francis, P., Galimberti, V., Gamal El Din Mohamed Mahmoud, H., Garber, J., Gnant, M., Gradishar, W., Gulluoglu, B., Harbeck, N., Huang, C.-S., Huober, J., Ilbawi, A., Jiang, Z., Johnston, S., Lee, E. S., Loibl, S., Morrow, M., Partridge, A., Piccart, M., Poortmans, P., Prat, A., Regan, M., Rubio, I., Rugo, H., Rutgers, E., Sedlmayer, F., Semiglazov, V., Senn, H.-J., Shao, Z., Spanic, T., Tesarova, P., Thürlimann, B., Tjulandin, S., Toi, M., Trudeau, M., Turner, N., Vaz Luis, I., Viale, G., Watanabe, T., Weber, W. P., Winer, E. P. & Xu, B. 2021. Customizing local and systemic therapies for women with early breast cancer: the St. Gallen International Consensus Guidelines for treatment of early breast cancer 2021. *Annals of Oncology,* 32**,** 1216-1235.

Byun, J. K., Lee, S., Kang, G. W., Lee, Y. R., Park, S. Y., Song, I. S., Yun, J. W., Lee, J., Choi, Y. K. & Park, K. G. 2022. Macropinocytosis is an alternative pathway of cysteine acquisition and mitigates sorafenib-induced ferroptosis in hepatocellular carcinoma. *J Exp Clin Cancer Res,* 41**,** 98.

Calzada-Fraile, D., Iborra, S., Ramírez-Huesca, M., Jorge, I., Dotta, E., Hernández-García, E., Martín-Cófreces, N., Nistal-Villán, E., Veiga, E., Vázquez, J., Pasqual, G. & Sánchez-Madrid, F. 2023. Immune synapse formation promotes lipid peroxidation and MHC-I upregulation in licensed dendritic cells for efficient priming of CD8(+) T cells. *Nat Commun,* 14**,** 6772.

Cano, A., Pérez-Moreno, M. A., Rodrigo, I., Locascio, A., Blanco, M. J., Del Barrio, M. G., Portillo, F. & Nieto, M. A. 2000. The transcription factor Snail controls epithelial–mesenchymal transitions by repressing E-cadherin expression. *Nature Cell Biology,* 2**,** 76-83.

Cardoso, F., Kyriakides, S., Ohno, S., Penault-Llorca, F., Poortmans, P., Rubio, I. T., Zackrisson, S. & Senkus, E. 2019. Early breast cancer: ESMO Clinical Practice Guidelines for diagnosis, treatment and follow-up[†]. *Annals of Oncology,* 30**,** 1194-1220.

Catanzaro, E., Demuynck, R., Naessens, F., Galluzzi, L. & Krysko, D. V. 2024. Immunogenicity of ferroptosis in cancer: a matter of context? *Trends in Cancer,* 10**,** 407-416.

Chen, Y. C., Sosnoski, D. M. & Mastro, A. M. 2010. Breast cancer metastasis to the bone: mechanisms of bone loss. *Breast Cancer Res,* 12**,** 215.

Chow, A., Zhou, W., Liu, L., Fong, M. Y., Champer, J., Van Haute, D., Chin, A. R., Ren, X., Gugiu, B. G., Meng, Z., Huang, W., Ngo, V., Kortylewski, M. & Wang, S. E. 2014. Macrophage immunomodulation by breast cancer-derived exosomes requires Toll-like receptor 2-mediated activation of NF-κB. *Sci Rep,* 4**,** 5750.

Cornel, A. M., Mimpen, I. L. & Nierkens, S. 2020. MHC Class I Downregulation in Cancer: Underlying Mechanisms and Potential Targets for Cancer Immunotherapy. *Cancers (Basel),* 12.

Croucher, P. I., Mcdonald, M. M. & Martin, T. J. 2016. Bone metastasis: the importance of the neighbourhood. *Nature Reviews Cancer,* 16**,** 373-386.

Dang, Q., Sun, Z., Wang, Y., Wang, L., Liu, Z. & Han, X. 2022. Ferroptosis: a double-edged sword mediating immune tolerance of cancer. *Cell Death & Disease,* 13**,** 925.

De Visser, K. E. & Joyce, J. A. 2023. The evolving tumor microenvironment: From cancer initiation to metastatic outgrowth. *Cancer Cell,* 41**,** 374-403.

Demuynck, R., Efimova, I., Naessens, F. & Krysko, D. V. 2021. Immunogenic ferroptosis and where to find it? *J Immunother Cancer,* 9.

Dent, R., Trudeau, M., Pritchard, K. I., Hanna, W. M., Kahn, H. K., Sawka, C. A., Lickley, L. A., Rawlinson, E., Sun, P. & Narod, S. A. 2007. Triple-Negative Breast Cancer: Clinical Features and Patterns of Recurrence. *Clinical Cancer Research,* 13**,** 4429-4434.

Dhatchinamoorthy, K., Colbert, J. D. & Rock, K. L. 2021. Cancer Immune Evasion Through Loss of MHC Class I Antigen Presentation. *Frontiers in Immunology,* Volume 12 - 2021.

Dierge, E., Debock, E., Guilbaud, C., Corbet, C., Mignolet, E., Mignard, L., Bastien, E., Dessy, C., Larondelle, Y. & Feron, O. 2021. Peroxidation of n-3 and n-6 polyunsaturated fatty acids in the acidic tumor environment leads to ferroptosis-mediated anticancer effects. *Cell Metabolism,* 33**,** 1701-1715.e5.

Dixon, Scott j., Lemberg, Kathryn m., Lamprecht, Michael r., Skouta, R., Zaitsev, Eleina m., Gleason, Caroline e., Patel, Darpan n., Bauer, Andras j., Cantley, Alexandra m., Yang, Wan s., Morrison, B., Iii & Stockwell, Brent r. 2012. Ferroptosis: An Iron-Dependent Form of Nonapoptotic Cell Death. *Cell,* 149**,** 1060-1072.

Doll, S., Proneth, B., Tyurina, Y. Y., Panzilius, E., Kobayashi, S., Ingold, I., Irmler, M., Beckers, J., Aichler, M., Walch, A., Prokisch, H., Trümbach, D., Mao, G., Qu, F., Bayir, H., Füllekrug, J., Scheel, C. H., Wurst, W., Schick, J. A., Kagan, V. E., Angeli, J. P. F. & Conrad, M. 2017. ACSL4 dictates ferroptosis sensitivity by shaping cellular lipid composition. *Nature Chemical Biology,* 13**,** 91-98.

Egeblad, M. & Werb, Z. 2002. New functions for the matrix metalloproteinases in cancer progression. *Nature Reviews Cancer,* 2**,** 161-174.

Feng, H., Schorpp, K., Jin, J., Yozwiak, C. E., Hoffstrom, B. G., Decker, A. M., Rajbhandari, P., Stokes, M. E., Bender, H. G., Csuka, J. M., Upadhyayula, P. S., Canoll, P., Uchida, K., Soni, R. K., Hadian, K. & Stockwell, B. R. 2020. Transferrin Receptor Is a Specific Ferroptosis Marker. *Cell Rep,* 30**,** 3411-3423.e7.

Fidler, I. J. 2003. The pathogenesis of cancer metastasis: the 'seed and soil' hypothesis revisited. *Nature Reviews Cancer,* 3**,** 453-458.

Folkman, J. 2002. Role of angiogenesis in tumor growth and metastasis. *Seminars in Oncology,* 29**,** 15-18.

Fukumura, D. & Jain, R. K. 2008. Imaging angiogenesis and the microenvironment. *APMIS,* 116**,** 695-715.

Galassi, C., Chan, T. A., Vitale, I. & Galluzzi, L. 2024. The hallmarks of cancer immune evasion. *Cancer Cell,* 42**,** 1825-1863.

Geyer, F. C., Pareja, F., Weigelt, B., Rakha, E., Ellis, I. O., Schnitt, S. J. & Reis-Filho, J. S. 2017. The Spectrum of Triple-Negative Breast Disease: High- and Low-Grade Lesions. *The American Journal of Pathology,* 187**,** 2139-2151.

Giles, A. J., Reid, C. M., Evans, J. D., Murgai, M., Vicioso, Y., Highfill, S. L., Kasai, M., Vahdat, L., Mackall, C. L., Lyden, D., Wexler, L. & Kaplan, R. N. 2016. Activation of Hematopoietic Stem/Progenitor Cells Promotes Immunosuppression Within the Pre-metastatic Niche. *Cancer Res,* 76**,** 1335-47.

Gong, T., Liu, L., Jiang, W. & Zhou, R. 2020. DAMP-sensing receptors in sterile inflammation and inflammatory diseases. *Nature Reviews Immunology,* 20**,** 95-112.

Gradishar, W. J., Moran, M. S., Abraham, J., Aft, R., Agnese, D., Allison, K. H., Anderson, B., Burstein, H. J., Chew, H., Dang, C., Elias, A. D., Giordano, S. H., Goetz, M. P., Goldstein, L. J., Hurvitz, S. A., Isakoff, S. J., Jankowitz, R. C., Javid, S. H., Krishnamurthy, J., Leitch, M., Lyons, J., Mortimer, J., Patel, S. A., Pierce, L. J., Rosenberger, L. H., Rugo, H. S., Sitapati, A., Smith, K. L., Smith, M. L., Soliman, H., Stringer-Reasor, E. M., Telli, M. L., Ward, J. H., Wisinski, K. B., Young, J. S., Burns, J. & Kumar, R. 2022. Breast Cancer, Version 3.2022, NCCN Clinical Practice Guidelines in Oncology. *Journal of the National Comprehensive Cancer Network,* 20**,** 691-722.

Guise, T. A., Mohammad, K. S., Clines, G., Stebbins, E. G., Wong, D. H., Higgins, L. S., Vessella, R., Corey, E., Padalecki, S., Suva, L. & Chirgwin, J. M. 2006. Basic Mechanisms Responsible for Osteolytic and Osteoblastic Bone Metastases. *Clinical Cancer Research,* 12**,** 6213s-6216s.

Guise, T. A. & Mundy, G. R. 1998. Cancer and Bone. *Endocrine Reviews,* 19**,** 18-54.

Hann, H.-W. L., Stahlhut, M. W. & Menduke, H. 1991. Iron enhances tumor growth. Observation on spontaneous mammary tumors in mice. *Cancer,* 68**,** 2407-2410.

Hiratsuka, S., Watanabe, A., Aburatani, H. & Maru, Y. 2006. Tumour-mediated upregulation of chemoattractants and recruitment of myeloid cells predetermines lung metastasis. *Nat Cell Biol,* 8**,** 1369-75.

Hong, X., Roh, W., Sullivan, R. J., Wong, K. H. K., Wittner, B. S., Guo, H., Dubash, T. D., Sade-Feldman, M., Wesley, B., Horwitz, E., Boland, G. M., Marvin, D. L., Bonesteel, T., Lu, C., Aguet, F., Burr, R., Freeman, S. S., Parida, L., Calhoun, K., Jewett, M. K., Nieman, L. T., Hacohen, N., Näär, A. M., Ting, D. T., Toner, M., Stott, S. L., Getz, G., Maheswaran, S. & Haber, D. A. 2021. The Lipogenic Regulator SREBP2 Induces Transferrin in Circulating Melanoma Cells and Suppresses Ferroptosis. *Cancer Discov,* 11**,** 678-695.

Hua, Y., Yang, S., Zhang, Y., Li, J., Wang, M., Yeerkenbieke, P., Liao, Q. & Liu, Q. 2024. Modulating ferroptosis sensitivity: environmental and cellular targets within the tumor microenvironment. *J Exp Clin Cancer Res,* 43**,** 19.

Huang, D. W., Sherman, B. T. & Lempicki, R. A. 2009. Systematic and integrative analysis of large gene lists using DAVID bioinformatics resources. *Nature Protocols,* 4**,** 44-57.

Kamińska, K., Szczylik, C., Bielecka, Z. F., Bartnik, E., Porta, C., Lian, F. & Czarnecka, A. M. 2015. The role of the cell-cell interactions in cancer progression. *J Cell Mol Med,* 19**,** 283-96.

Kang, Y., Siegel, P. M., Shu, W., Drobnjak, M., Kakonen, S. M., Cordón-Cardo, C., Guise, T. A. & Massagué, J. 2003. A multigenic program mediating breast cancer metastasis to bone. *Cancer Cell,* 3**,** 537-549.

Karaman, S. & Detmar, M. 2014. Mechanisms of lymphatic metastasis. *The Journal of Clinical Investigation,* 124**,** 922-928.

Kim, J., Harper, A., Mccormack, V., Sung, H., Houssami, N., Morgan, E., Mutebi, M., Garvey, G., Soerjomataram, I. & Fidler-Benaoudia, M. M. 2025. Global patterns and trends in breast cancer incidence and mortality across 185 countries. *Nature Medicine,* 31**,** 1154-1162.

Kim, K. J., Li, B., Winer, J., Armanini, M., Gillett, N., Phillips, H. S. & Ferrara, N. 1993. Inhibition of vascular endothelial growth factor-induced angiogenesis suppresses tumour growth in vivo. *Nature,* 362**,** 841-844.

Klymkowsky, M. W. & Savagner, P. 2009. Epithelial-Mesenchymal Transition: A Cancer Researcher's Conceptual Friend and Foe. *The American Journal of Pathology,* 174**,** 1588-1593.
Kolb, A. D. & Bussard, K. M. 2019. The Bone Extracellular Matrix as an Ideal Milieu for Cancer Cell Metastases. *Cancers,* 11**,** 1020.
Kong, S., Zhang, J., Wang, L., Li, W., Guo, H., Weng, Q., He, Q., Lou, H., Ding, L. & Yang, B. 2025. Mechanisms of low MHC I expression and strategies for targeting MHC I with small molecules in cancer immunotherapy. *Cancer Letters,* 611**,** 217432.
Koyama, M. & Hill, G. R. 2021. Mouse Models of Antigen Presentation in Hematopoietic Stem Cell Transplantation. *Frontiers in Immunology,* Volume 12 - 2021.
Kwa, M. J. & Adams, S. 2018. Checkpoint inhibitors in triple-negative breast cancer (TNBC): Where to go from here. *Cancer,* 124**,** 2086-2103.
Lambert, A. W., Pattabiraman, D. R. & Weinberg, R. A. 2017. Emerging Biological Principles of Metastasis. *Cell,* 168**,** 670-691.
Larraufie, M. H., Yang, W. S., Jiang, E., Thomas, A. G., Slusher, B. S. & Stockwell, B. R. 2015. Incorporation of metabolically stable ketones into a small molecule probe to increase potency and water solubility. *Bioorg Med Chem Lett,* 25**,** 4787-4792.
Lei, G., Zhuang, L. & Gan, B. 2022a. Targeting ferroptosis as a vulnerability in cancer. *Nat Rev Cancer,* 22**,** 381-396.
Lei, X., Lin, H., Wang, J., Ou, Z., Ruan, Y., Sadagopan, A., Chen, W., Xie, S., Chen, B., Li, Q., Wang, J., Lin, H., Zhu, X., Yuan, X., Tian, T., Lv, X., Fu, S., Zhu, X., Zhou, J., Pan, G., Xia, X., Tannous, B. A., Ferrone, S., Fan, S. & Li, J. 2022b. Mitochondrial fission induces immunoescape in solid tumors through decreasing MHC-I surface expression. *Nat Commun,* 13**,** 3882.
Li, L., Bo, Y., Xue, D. & Qin, L. 2025. Ferroptosis-immune crosstalk in cervical cancer: mechanisms and therapeutic implications. *Front Immunol,* 16.
Lin, N. U., Vanderplas, A., Hughes, M. E., Theriault, R. L., Edge, S. B., Wong, Y.-N., Blayney, D. W., Niland, J. C., Winer, E. P. & Weeks, J. C. 2012. Clinicopathologic features, patterns of recurrence, and survival among women with triple-negative breast cancer in the National Comprehensive Cancer Network. *Cancer,* 118**,** 5463-5472.
Litton, J. K., Rugo, H. S., Ettl, J., Hurvitz, S. A., Gonçalves, A., Lee, K.-H., Fehrenbacher, L., Yerushalmi, R., Mina, L. A., Martin, M., Roché, H., Im, Y.-H., Quek, R. G. W., Markova, D., Tudor, I. C., Hannah, A. L., Eiermann, W. & Blum, J. L. 2018. Talazoparib in Patients with Advanced Breast Cancer and a Germline BRCA Mutation. *New England Journal of Medicine,* 379**,** 753-763.
Lorito, N., Subbiani, A., Smiriglia, A., Bacci, M., Bonechi, F., Tronci, L., Romano, E., Corrado, A., Longo, D. L., Iozzo, M., Ippolito, L., Comito, G., Giannoni, E., Meattini, I., Avgustinova, A., Chiarugi, P., Bachi, A. & Morandi, A. 2024. FADS1/2 control lipid metabolism and ferroptosis susceptibility in triple-negative breast cancer. *EMBO Molecular Medicine,* 16**,** 1533-1559-1559.
Ma, X., Xiao, L., Liu, L., Ye, L., Su, P., Bi, E., Wang, Q., Yang, M., Qian, J. & Yi, Q. 2021. CD36-mediated ferroptosis dampens intratumoral $CD8^+$ T cell effector function and impairs their antitumor ability. *Cell Metabolism,* 33**,** 1001-1012.e5.
Macedo, F., Ladeira, K., Pinho, F., Saraiva, N., Bonito, N., Pinto, L. & Goncalves, F. 2017. Bone Metastases: An Overview. *Oncol Rev,* 11**,** 321.
Maeda, H. 2001. The enhanced permeability and retention (EPR) effect in tumor vasculature: the key role of tumor-selective macromolecular drug targeting. *Advances in Enzyme Regulation,* 41**,** 189-207.
Maeurer, M. J., Gollin, S. M., Storkus, W. J., Swaney, W., Karbach, J., Martin, D., Castelli, C., Salter, R., Knuth, A. & Lotze, M. T. 1996. Tumor escape from immune recognition: loss of HLA-A2 melanoma cell surface expression is associated with a complex rearrangement of the short arm of chromosome 6. *Clinical Cancer Research,* 2**,** 641-652.

Mandriota, S. J., Jussila, L., Jeltsch, M., Compagni, A., Baetens, D., Prevo, R., Banerji, S., Huarte, J., Montesano, R., Jackson, D. G., Orci, L., Alitalo, K., Christofori, G. & Pepper, M. S. 2001. Vascular endothelial growth factor-C-mediated lymphangiogenesis promotes tumour metastasis. *The EMBO Journal,* 20**,** 672-682.

Mani, S. A., Yang, J., Brooks, M., Schwaninger, G., Zhou, A., Miura, N., Kutok, J. L., Hartwell, K., Richardson, A. L. & Weinberg, R. A. 2007. Mesenchyme Forkhead 1 (FOXC2) plays a key role in metastasis and is associated with aggressive basal-like breast cancers. *Proceedings of the National Academy of Sciences,* 104**,** 10069-10074.

Marcus, D. M. & Zinberg, N. 1975. Measurement of Serum Ferritin by Radioimmunoassay: Results in Normal Individuals and Patients With Breast Cancer2. *JNCI: Journal of the National Cancer Institute,* 55**,** 791-795.

Massagué, J. & Obenauf, A. C. 2016. Metastatic colonization by circulating tumour cells. *Nature,* 529**,** 298-306.

Medeiros, B. & Allan, A. L. 2019. Molecular Mechanisms of Breast Cancer Metastasis to the Lung: Clinical and Experimental Perspectives. *Int J Mol Sci,* 20.

Minn, A. J., Gupta, G. P., Siegel, P. M., Bos, P. D., Shu, W., Giri, D. D., Viale, A., Olshen, A. B., Gerald, W. L. & Massagué, J. 2005. Genes that mediate breast cancer metastasis to lung. *Nature,* 436**,** 518-524.

Nassar, Z. D., Mah, C. Y., Dehairs, J., Burvenich, I. J., Irani, S., Centenera, M. M., Helm, M., Shrestha, R. K., Moldovan, M., Don, A. S., Holst, J., Scott, A. M., Horvath, L. G., Lynn, D. J., Selth, L. A., Hoy, A. J., Swinnen, J. V. & Butler, L. M. 2020. Human DECR1 is an androgen-repressed survival factor that regulates PUFA oxidation to protect prostate tumor cells from ferroptosis. *Elife,* 9.

Page, J. M., Merkel, A. R., Ruppender, N. S., Guo, R., Dadwal, U. C., Cannonier, S., Basu, S., Guelcher, S. A. & Sterling, J. A. 2015. Matrix rigidity regulates the transition of tumor cells to a bone-destructive phenotype through integrin β3 and TGF-β receptor type II. *Biomaterials,* 64**,** 33-44.

Paget, S. 1889. The distribution of secondary growths in cancer of the breast. *The Lancet,* 133**,** 571-573.

Pedersen, M. H., Hood, B. L., Beck, H. C., Conrads, T. P., Ditzel, H. J. & Leth-Larsen, R. 2017. Downregulation of antigen presentation-associated pathway proteins is linked to poor outcome in triple-negative breast cancer patient tumors. *Oncoimmunology,* 6**,** e1305531.

Peng, F., Liao, M., Qin, R., Zhu, S., Peng, C., Fu, L., Chen, Y. & Han, B. 2022. Regulated cell death (RCD) in cancer: key pathways and targeted therapies. *Signal Transduction and Targeted Therapy,* 7**,** 286.

Polyak, K. & Weinberg, R. A. 2009. Transitions between epithelial and mesenchymal states: acquisition of malignant and stem cell traits. *Nature Reviews Cancer,* 9**,** 265-273.

Poznanski, S. M., Singh, K., Ritchie, T. M., Aguiar, J. A., Fan, I. Y., Portillo, A. L., Rojas, E. A., Vahedi, F., El-Sayes, A., Xing, S., Butcher, M., Lu, Y., Doxey, A. C., Schertzer, J. D., Hirte, H. W. & Ashkar, A. A. 2021. Metabolic flexibility determines human NK cell functional fate in the tumor microenvironment. *Cell Metabolism,* 33**,** 1205-1220.e5.

Ramakrishnan, R., Tyurin, V. A., Veglia, F., Condamine, T., Amoscato, A., Mohammadyani, D., Johnson, J. J., Zhang, L. M., Klein-Seetharaman, J., Celis, E., Kagan, V. E. & Gabrilovich, D. I. 2014. Oxidized lipids block antigen cross-presentation by dendritic cells in cancer. *J Immunol,* 192**,** 2920-31.

Rankin, E. B., Nam, J.-M. & Giaccia, A. J. 2016. Hypoxia: Signaling the Metastatic Cascade. *Trends in Cancer,* 2**,** 295-304.

Riemann, A., Schneider, B., Gündel, D., Stock, C., Gekle, M. & Thews, O. Acidosis Promotes Metastasis Formation by Enhancing Tumor Cell Motility. *In:* ELWELL, C.

E., LEUNG, T. S. & HARRISON, D. K., eds. Oxygen Transport to Tissue XXXVII, 2016// 2016 New York, NY. Springer New York, 215-220.
Robson, M., Im, S.-A., Senkus, E., Xu, B., Domchek, S. M., Masuda, N., Delaloge, S., Li, W., Tung, N., Armstrong, A., Wu, W., Goessl, C., Runswick, S. & Conte, P. 2017. Olaparib for Metastatic Breast Cancer in Patients with a Germline BRCA Mutation. *New England Journal of Medicine,* 377**,** 523-533.
Schild, T., Low, V., Blenis, J. & Gomes, A. P. 2018. Unique Metabolic Adaptations Dictate Distal Organ-Specific Metastatic Colonization. *Cancer Cell,* 33**,** 347-354.
Schwab, A., Rao, Z., Zhang, J., Gollowitzer, A., Siebenkäs, K., Bindel, N., D'avanzo, E., Van Roey, R., Hajjaj, Y., Özel, E., Armstark, I., Bereuter, L., Su, F., Grander, J., Bonyadi Rad, E., Groenewoud, A., Engel, F. B., Bell, G. W., Henry, W. S., Angeli, J. P. F., Stemmler, M. P., Brabletz, S., Koeberle, A. & Brabletz, T. 2024. Zeb1 mediates EMT/plasticity-associated ferroptosis sensitivity in cancer cells by regulating lipogenic enzyme expression and phospholipid composition. *Nature Cell Biology,* 26**,** 1470-1481.
Seager, R. J., Hajal, C., Spill, F., Kamm, R. D. & Zaman, M. H. 2017. Dynamic interplay between tumour, stroma and immune system can drive or prevent tumour progression. *Converg Sci Phys Oncol,* 3.
Shen, M. & Kang, Y. 2020. Stresses in the metastatic cascade: molecular mechanisms and therapeutic opportunities. *Genes Dev,* 34**,** 1577-1598.
Siegel, R. L., Kratzer, T. B., Giaquinto, A. N., Sung, H. & Jemal, A. 2025. Cancer statistics, 2025. *CA: A Cancer Journal for Clinicians,* 75**,** 10-45.
Sotiriou, C., Lacroix, M., Lespagnard, L., Larsimont, D., Paesmans, M. & Body, J.-J. 2001. Interleukins-6 and -11 expression in primary breast cancer and subsequent development of bone metastases. *Cancer Letters,* 169**,** 87-95.
Stevens, T., Phan, S., Frid, M. G., Alvarez, D., Herzog, E. & Stenmark, K. R. 2008. Lung Vascular Cell Heterogeneity. *Proceedings of the American Thoracic Society,* 5**,** 783-791.
Su, Z., Yang, Z., Xu, Y., Chen, Y. & Yu, Q. 2015. Apoptosis, autophagy, necroptosis, and cancer metastasis. *Molecular Cancer,* 14**,** 48.
Taichman, R. S., Cooper, C., Keller, E. T., Pienta, K. J., Taichman, N. S. & Mccauley, L. K. 2002. Use of the stromal cell-derived factor-1/CXCR4 pathway in prostate cancer metastasis to bone. *Cancer Res,* 62**,** 1832-7.
Tan, P. H., Ellis, I., Allison, K., Brogi, E., Fox, S. B., Lakhani, S., Lazar, A. J., Morris, E. A., Sahin, A., Salgado, R., Sapino, A., Sasano, H., Schnitt, S., Sotiriou, C., Van Diest, P., White, V. A., Lokuhetty, D., Cree, I. A. & Board, F. T. W. C. O. T. E. 2020. The 2019 World Health Organization classification of tumours of the breast. *Histopathology,* 77**,** 181-185.
Tang, D., Chen, M., Huang, X., Zhang, G., Zeng, L., Zhang, G., Wu, S. & Wang, Y. 2023. SRplot: A free online platform for data visualization and graphing. *PLOS ONE,* 18**,** e0294236.
Taube, J. H., Herschkowitz, J. I., Komurov, K., Zhou, A. Y., Gupta, S., Yang, J., Hartwell, K., Onder, T. T., Gupta, P. B., Evans, K. W., Hollier, B. G., Ram, P. T., Lander, E. S., Rosen, J. M., Weinberg, R. A. & Mani, S. A. 2010. Core epithelial-to-mesenchymal transition interactome gene-expression signature is associated with claudin-low and metaplastic breast cancer subtypes. *Proceedings of the National Academy of Sciences,* 107**,** 15449-15454.
Taylor, B. C. & Balko, J. M. 2022. Mechanisms of MHC-I Downregulation and Role in Immunotherapy Response. *Frontiers in Immunology,* 13.
Torti, S. V., Manz, D. H., Paul, B. T., Blanchette-Farra, N. & Torti, F. M. 2018. Iron and Cancer. *Annu Rev Nutr,* 38**,** 97-125.
Ubellacker, J. M., Tasdogan, A., Ramesh, V., Shen, B., Mitchell, E. C., Martin-Sandoval, M. S., Gu, Z., Mccormick, M. L., Durham, A. B., Spitz, D. R., Zhao, Z., Mathews, T. P. & Morrison, S. J. 2020. Lymph protects metastasizing melanoma cells from ferroptosis. *Nature,* 585**,** 113-118.

Verma, N., Vinik, Y., Saroha, A., Nair, N. U., Ruppin, E., Mills, G., Karn, T., Dubey, V., Khera, L., Raj, H., Maina, F. & Lev, S. 2020. Synthetic lethal combination targeting BET uncovered intrinsic susceptibility of TNBC to ferroptosis. *Science Advances,* 6**,** eaba8968.

Viswanathan, V. S., Ryan, M. J., Dhruv, H. D., Gill, S., Eichhoff, O. M., Seashore-Ludlow, B., Kaffenberger, S. D., Eaton, J. K., Shimada, K., Aguirre, A. J., Viswanathan, S. R., Chattopadhyay, S., Tamayo, P., Yang, W. S., Rees, M. G., Chen, S., Boskovic, Z. V., Javaid, S., Huang, C., Wu, X., Tseng, Y.-Y., Roider, E. M., Gao, D., Cleary, J. M., Wolpin, B. M., Mesirov, J. P., Haber, D. A., Engelman, J. A., Boehm, J. S., Kotz, J. D., Hon, C. S., Chen, Y., Hahn, W. C., Levesque, M. P., Doench, J. G., Berens, M. E., Shamji, A. F., Clemons, P. A., Stockwell, B. R. & Schreiber, S. L. 2017. Dependency of a therapy-resistant state of cancer cells on a lipid peroxidase pathway. *Nature,* 547**,** 453-457.

Waks, A. G. & Winer, E. P. 2019. Breast Cancer Treatment: A Review. *JAMA,* 321**,** 288-300.

Weidner, N., Semple, J. P., Welch, W. R. & Folkman, J. 1991. Tumor Angiogenesis and Metastasis — Correlation in Invasive Breast Carcinoma. *New England Journal of Medicine,* 324**,** 1-8.

Wiernicki, B., Maschalidi, S., Pinney, J., Adjemian, S., Vanden Berghe, T., Ravichandran, K. S. & Vandenabeele, P. 2022. Cancer cells dying from ferroptosis impede dendritic cell-mediated anti-tumor immunity. *Nature Communications,* 13**,** 3676.

Winkler, J., Abisoye-Ogunniyan, A., Metcalf, K. J. & Werb, Z. 2020. Concepts of extracellular matrix remodelling in tumour progression and metastasis. *Nature Communications,* 11**,** 5120.

World Health Organization 2025. Breast cancer.

Wu, H., Zhang, J., Dai, R., Xu, J. & Feng, H. 2019. Transferrin receptor-1 and VEGF are prognostic factors for osteosarcoma. *J Orthop Surg Res,* 14**,** 296.

Wu, J., Fan, D., Shao, Z., Xu, B., Ren, G., Jiang, Z., Wang, Y., Jin, F., Zhang, J., Zhang, Q., Ma, F., Ma, J., Wang, Z., Wang, S., Wang, X., Wang, S., Wang, H., Wang, T., Wang, X., Wang, J., Wang, J., Wang, B., Fu, L., Li, H., Shi, Y., Gan, L., Liu, Y., Liu, J., Liu, Z., Liu, Q., Sun, Q., Cheng, W., Yu, K., Tong, Z., Wu, X., Song, C., Zhang, J., Zhang, J., Li, J., Li, B., Li, M., Li, H., Yang, W., Yang, H., Yang, B., Bu, H., Shen, J., Shen, Z., Chen, Y., Chen, C., Pang, D., Fan, Z., Zheng, Y., Yu, X., Liu, G., Hu, X., Ling, Y., Tang, J., Yin, Y., Geng, C., Yuan, P., Gu, Y., Chang, C., Cao, X., Sheng, Y., Huang, Y., Huang, J., Peng, W., Zeng, X., Xie, Y., Liao, N., Daiming, F., Zhimin, S., Binghe, X., Guosheng, R., Jiong, W., Zefei, J., Yongsheng, W., Feng, J., Jin, Z., Qingyuan, Z., Fei, M., Jinli, M., Zhonghua, W., Yongsheng, W., Shusen, W., Xiaojia, W., Shu, W., Haibo, W., Tao, W., Xiang, W., Jing, W., Jia, W., Biyun, W., Li, F., Hongyuan, L., Yehui, S., Lu, G., Guosheng, R., Yunjiang, L., et al. 2022. CACA Guidelines for Holistic Integrative Management of Breast Cancer. *Holistic Integrative Oncology,* 1**,** 7.

Wu, S., Ge, A., Deng, X., Liu, L. & Wang, Y. 2024. Evolving immunotherapeutic solutions for triple-negative breast carcinoma. *Cancer Treatment Reviews,* 130**,** 102817.

Xiang, X., Poliakov, A., Liu, C., Liu, Y., Deng, Z. B., Wang, J., Cheng, Z., Shah, S. V., Wang, G. J., Zhang, L., Grizzle, W. E., Mobley, J. & Zhang, H. G. 2009. Induction of myeloid-derived suppressor cells by tumor exosomes. *Int J Cancer,* 124**,** 2621-33.

Xiao, W., Zheng, S., Liu, P., Zou, Y., Xie, X., Yu, P., Tang, H. & Xie, X. 2018. Risk factors and survival outcomes in patients with breast cancer and lung metastasis: a population-based study. *Cancer Med,* 7**,** 922-930.

Yang, J., Mani, S. A., Donaher, J. L., Ramaswamy, S., Itzykson, R. A., Come, C., Savagner, P., Gitelman, I., Richardson, A. & Weinberg, R. A. 2004. Twist, a Master Regulator of Morphogenesis, Plays an Essential Role in Tumor Metastasis. *Cell,* 117**,** 927-939.

Yang, K., Halima, A. & Chan, T. A. 2023. Antigen presentation in cancer — mechanisms and clinical implications for immunotherapy. *Nature Reviews Clinical Oncology,* 20**,** 604-623.

Yang, Wan s., Sriramaratnam, R., Welsch, Matthew e., Shimada, K., Skouta, R., Viswanathan, Vasanthi s., Cheah, Jaime h., Clemons, Paul a., Shamji, Alykhan f., Clish, Clary b., Brown, Lewis m., Girotti, Albert w., Cornish, Virginia w., Schreiber, Stuart l. & Stockwell, Brent r. 2014. Regulation of Ferroptotic Cancer Cell Death by GPX4. *Cell,* 156**,** 317-331.

Yuan, J., Liu, C., Jiang, C., Liu, N., Yang, Z. & Xing, H. 2025. RSL3 induces ferroptosis by activating the NF-κB signalling pathway to enhance the chemosensitivity of triple-negative breast cancer cells to paclitaxel. *Scientific Reports,* 15**,** 1654.

Zhang, C., Zhang, L., Xu, T., Xue, R., Yu, L., Zhu, Y., Wu, Y., Zhang, Q., Li, D., Shen, S., Tan, D., Bai, F. & Zhang, H. 2020. Mapping the spreading routes of lymphatic metastases in human colorectal cancer. *Nature Communications,* 11**,** 1993.

Zhang, H. F., Klein Geltink, R. I., Parker, S. J. & Sorensen, P. H. 2022. Transsulfuration, minor player or crucial for cysteine homeostasis in cancer. *Trends Cell Biol,* 32**,** 800-814.

Zhang, J., Goliwas, K. F., Wang, W., Taufalele, P. V., Bordeleau, F. & Reinhart-King, C. A. 2019a. Energetic regulation of coordinated leader–follower dynamics during collective invasion of breast cancer cells. *Proceedings of the National Academy of Sciences,* 116**,** 7867-7872.

Zhang, R., Chen, J., Wang, S., Zhang, W., Zheng, Q. & Cai, R. 2023. Ferroptosis in Cancer Progression. *Cells,* 12.

Zhang, Y., Tan, H., Daniels, J. D., Zandkarimi, F., Liu, H., Brown, L. M., Uchida, K., O'connor, O. A. & Stockwell, B. R. 2019b. Imidazole Ketone Erastin Induces Ferroptosis and Slows Tumor Growth in a Mouse Lymphoma Model. *Cell Chemical Biology,* 26**,** 623-633.e9.

Zou, Y. & Schreiber, S. L. 2020. Progress in Understanding Ferroptosis and Challenges in Its Targeting for Therapeutic Benefit. *Cell Chem Biol,* 27**,** 463-471.